Journal of Non-Newtonian Fluid Mechanics 166 (2011) 639–660

Contents lists available at ScienceDirect

Journal of Non-Newtonian Fluid Mechanics

journal homepage: http://www.elsevier.com/locate/jnnfm

A FENE-P k–ε turbulence model for low and intermediate regimes of polymer-induced drag reduction

P.R. Resende [a,b], K. Kim [c], B.A. Younis [d], R. Sureshkumar [e], F.T. Pinho [a,*]

[a] Departamento de Engenharia Mecânica, CEFT, Faculdade de Engenharia da Universidade do Porto, Rua Dr. Roberto Frias s/n, 4200-465 Porto, Portugal
[b] Escola Superior de Estudos Industriais e de Gestão, Instituto Politécnico do Porto, Rua D. Sancho I, 981, 4480-876 Vila do Conde, Portugal
[c] Department of Mechanical Engineering, Hanbat National University, Daejeon 305-719, South Korea
[d] Department of Civil and Environmental Engineering, University of California, Davis, CA 95616, USA
[e] Department of Biomedical and Chemical Engineering, Department of Physics, Syracuse University, NY 13244, USA

ARTICLE INFO

Article history:
Received 27 May 2010
Received in revised form 14 January 2011
Accepted 28 February 2011
Available online 12 April 2011

Keywords:
RANS
Turbulence model
Polymer drag reduction
FENE-P
Viscoelastic

ABSTRACT

A new low-Reynolds-number k–ε turbulence model is developed for flows of viscoelastic fluids described by the finitely extensible nonlinear elastic rheological constitutive equation with Peterlin approximation (FENE-P model). The model is validated against direct numerical simulations in the low and intermediate drag reduction (DR) regimes (DR up to 50%). The results obtained represent an improvement over the low DR model of Pinho et al. (2008) [A low Reynolds number k–ε turbulence model for FENE-P viscoelastic fluids, Journal of Non-Newtonian Fluid Mechanics, 154, 89–108]. In extending the range of application to higher values of drag reduction, three main improvements were incorporated: a modified eddy viscosity closure, the inclusion of direct viscoelastic contributions into the transport equations for turbulent kinetic energy (k) and its dissipation rate, and a new closure for the cross-correlations between the fluctuating components of the polymer conformation and rate of strain tensors (NLT_{ij}). The NLT_{ij} appears in the Reynolds-averaged evolution equation for the conformation tensor (RACE), which is required to calculate the average polymer stress, and in the viscoelastic stress work in the transport equation of k. It is shown that the predictions of mean velocity, turbulent kinetic energy, its rate of dissipation by the Newtonian solvent, conformation tensor and polymer and Reynolds shear stresses are improved compared to those obtained from the earlier model.

1. Introduction

It is well known that the addition of small amounts of additives that impart viscoelastic properties to fluids can represent an effective way to reduce drag and heat transfer [1–4]. These early studies were aimed at quantifying the relationship between fluid rheology, polymer molecular weight and concentration on one side and drag reduction (DR), Reynolds stresses and velocity profiles on the other. These studies, which were experimental or numerical using direct numerical simulations (DNS) increased significantly our phenomenological understanding of drag reduction. Nevertheless, and despite the increase in computational power, our predictive capability of non-Newtonian viscoelastic turbulent flows remains very limited. This has motivated the use of direct numerical simulation of viscoelastic turbulent flow in simple geometries such as the plane channel [3,5,6] to assess the performance of turbulence closures intended for use in the more complicated flows encountered in industrial applications [7–9].

The earlier attempts to develop turbulence closures for non-Newtonian fluids had no link with fluid rheology and essentially showed that it was possible to predict drag reduction (DR) by a suitable modification of the von Kármán coefficient [10]. An exception was the simple eddy viscosity model of Mizushina and Usui [11], which used a Van Driest damping function modified to incorporate a coefficient related nonlinearly, and with a very large coefficient of the order of 10^8, to the relaxation time of the linear viscoelastic Rouse model. More recent turbulence models included only variable viscosity effects, described by such rheological constitutive equations as the power law or Bingham law for yield-stress fluids [12,13]. In an attempt to incorporate viscoelastic fluid rheology into turbulence models for drag reducing fluids, Pinho and co-workers [14–17] developed several first-order turbulence models for a modified version of the generalised Newtonian fluid constitutive equation, where the dependence of strain hardening of the fluid on the third invariant of the rate of deformation tensor was included. These models also included an anisotropic version to capture the increased Reynolds stress anisotropy [17]. However,

* Corresponding author.
E-mail addresses: resende@fe.up.pt (P.R. Resende), kkim@hanbat.ac.kr (K. Kim), bayounis@ucdavis.edu (B.A. Younis), rsureshk@syr.edu (R. Sureshkumar), fpinho@fe.up.pt (F.T. Pinho).

0377-0257/$ - see front matter © 2011 Elsevier B.V. All rights reserved.
doi:10.1016/j.jnnfm.2011.02.012

this constitutive equation is not truly elastic in nature, therefore it is unable to capture important features of elastic fluids, namely the memory effect and its spatio-temporal variation. To illustrate this feature, using a simplified version of the second order fluid equation, Pinho et al. [18] derived a simple one-equation k–l turbulence model that was capable of predicting drag reduction by incorporating the time-average elastic shear stress in the momentum equation. This feature especially required a closure for the elastic stress work (interaction between fluctuating elastic stress and rate of strain tensors) appearing in the transport equation for turbulence kinetic energy, provided the elastic stress work was mostly dissipative. The adoption of a viscoelastic constitutive equation including memory effects, such as the finitely extensible nonlinear elastic model with Peterlin's modification (FENE-P), was the obvious choice given the availability of DNS data.

The ability to accurately predict the flow characteristics of viscoelastic fluids in complicated geometries is important for the design and optimisation of engineering applications, e.g., use of drag reducing agents in geometries with bends, bifurcations and expansions/contractions of the flow cross-section. To date, this ability is very limited. The DNS predictions of viscoelastic turbulent flows by Dimitropoulos et al. [19], Housiadas et al. [6] and Li et al. [8], amongst others, give insight into the physics of drag reduction by polymer additives, while providing useful data for developing suitable turbulence models. We also note that the latter work includes a zero-order eddy viscosity closure. The FENE-P model was used to describe fluid rheology in the above studies although some research has also been carried out with the Oldroyd-B and Giesekus models [20,21]. The use of DNS for engineering calculations is prohibitively expensive and hence the need to resort to the methodologies of large eddy simulation (LES) or RANS methods. The latter is adopted in this work and follows, with the necessary adaptations, the work developed by Pinho and co-workers [15–17] for a modified generalised Newtonian fluid model.

As mentioned, the constitutive equation used in [14–16] lacked memory effects. Constitutive equations based on polymer kinetic theory, such as the FENE-P model, are physically more realistic in their description of the rheology of the dilute and semi-dilute polymer solutions. However, as pointed out by Ptasinski et al. [22] there is a quantitative discrepancy between the experimentally measured and numerically predicted (by DNS) amounts of drag reduction when using the FENE-P model with the relaxation time measured in shear rheology. This is due to one of several reasons. As Gupta et al. [23] point out, part of the issue is related to the closure inherent to the FENE-P constitutive equation. Its predictions could be improved by suitably renormalising the extensibility parameter in the model or by using a different FENE closure [24]. Another cause of discrepancy is the simplicity of the underlying dumbbell model, namely the lack of configurational degrees of freedom. On the experimental side, concentration effects and polymer degradation effects can be very intense, especially when using low concentrations of flexible polymers with a very high molecular weight [25,26]. Nevertheless, the DNS predictions are qualitatively correct and provide consistent and physically meaningful depictions of the energy transfer mechanisms in turbulent polymer drag reduction [6,27–29].

In addition to the zero-order eddy viscosity model of Li et al. [8], there have been some other attempts at developing RANS/RACE turbulence closures for the FENE-P fluid (RACE stands for Reynolds-averaged conformation equation). Leighton et al. [7,30] proposed a second-order Reynolds stress model in which closure approximations were put forward for the fluctuating pressure-strain term and for the new terms containing the interactions between fluctuations of the polymer stress and kinematic quantities. Shaqfeh et al. [31] modified the v^2-f model of Durbin [32] by relating the time-averaged polymer stress as a function of the conformation, as is obvious from its evolution equation, but in a simplified manner by invoking exclusively the relevance of extensional flow. As a consequence, instead of working with the full conformation tensor, only an equation for its trace is required. The time average polymer stress is then modelled in a Boussinesq-like form introducing the concept of turbulent viscoelastic viscosity. They also introduced changes to the transport equations for k and v^2, where the pressure-strain term was modified to depend on viscoelastic quantities. At the end, and even though the model contains only three new coefficients and captures well the velocity profiles at low and high drag reductions (LDR and HDR, respectively), it underpredicts the distribution of turbulent kinetic energy and overpredicts mean polymer elongation.

Recently, in their development of a k–ε model for FENE-P fluids, Pinho et al. [9] used the Reynolds-averaged form of the conformation tensor equation to determine the average polymer stress. The outcome was a simple closure for the nonlinear tensor term that quantifies the cross-correlation between the fluctuating conformation and velocity gradient tensors arising from the distortion term of Oldroyd's upper convective derivative, hereafter referred to as NLT_{ij} (defined in Eq. (11)). Further, they developed accurate closures for the viscoelastic stress work and for the viscoelastic – turbulent diffusion appearing in the equation for k. Since the model was calibrated using only low drag reduction DNS data, it was unable to predict higher drag reductions. The model also had deficiencies in predicting accurately secondary quantities such as the rate of dissipation of turbulent kinetic energy, but to our knowledge it is still the only existing first-order closure for a FENE-P fluid which is extensively documented in the archival literature.

In the context of single point closures, the Reynolds-averaged evolution equation for the conformation tensor (C_{ij}) contains the new term NLT_{ij} that requires closure so that the average polymer stress contribution to the turbulent momentum balance can be calculated. However, the relevance of NLT_{ij} is not limited to the evolution equation of the conformation tensor. As shown by Pinho et al. [9], NLT_{ij} and its trace also appear in closures developed for the viscoelastic stress work term of the transport equations of the Reynolds stresses and of the turbulent kinetic energy for viscoelastic fluids, respectively. The closure for the viscoelastic stress work developed in [9] was tested against DNS data for low drag reduction. An essential step in devising a more generally applicable single point turbulence model for viscoelastic fluids described by the FENE-P rheological equation of state is the development of a more accurate closure for NLT_{ij}, which is one of the aims of this work.

In their previous investigation, Pinho et al. [9] devised a simple model for NLT_{ij} based on a functional single-point relationship between this tensor and the set of parameters on which it depends. This functional relationship was reduced through the application of the principles of symmetry, invariance, permutation and realizability as inspired by Younis et al. [33,34], but there could be still some problems of invariance due to the use of the vorticity tensor, which we address in the present development. Besides, the model derived in [9] was limited to low drag reduction (DR < 30%) and was unable to capture some of the features of the NLT_{ij} tensor, such as the negative peak of NLT_{11} at the buffer layer, and it underestimated NLT_{33}. The new closure for NLT_{ij} presented here is derived from its exact equation using physical insight from post-processed DNS data, order of magnitude analysis of terms and arguments from homogeneous isotropic turbulence. Here, the closures are extended to the intermediate drag reduction (IDR) regime (this corresponds to the low end of the high drag reduction regime, up to DR $\approx$50%). Specifically, additional modifications to the original model of Pinho et al. [9] include the direct incorporation of viscoelastic properties into the eddy viscosity model for the Reynolds stresses

and the transport equation for the rate of dissipation of turbulence by the Newtonian solvent, which must necessarily be affected by the presence of polymer additives. Some of the closures developed by Pinho et al. [9] were also revisited, since the relative contributions of the double and triple correlations to the closures in the IDR regime differ from those at LDR.

The paper is organised as follows: the Reynolds-average governing equations for the turbulent flow of FENE-P fluids are presented in Section 2. Section 3 describes how the exact equation for NLT_{ij} is derived and then presents and justifies an approximation to this exact equation from which the closure is developed. The Reynolds stress and the viscoelastic closures specific to the transport equations of k and of its rate of dissipation by the Newtonian solvent (ε^N) are treated in Section 4, which also includes the extension of the model for the viscoelastic stress work of Pinho et al. [9] to the IDR regime. After remembering the final set of governing equations that need to be solved, the paper presents predictions by the new viscoelastic turbulence model and assesses its performance against DNS data. Finally, the paper closes with the main conclusions and recommendations for future work.

2. Governing equations and non-dimensional numbers

In what follows, uppercase letters and overbars denote Reynolds-averaged quantities, whereas lowercase letters and primes denote fluctuations. A caret is used to identify instantaneous quantities. Conventional Cartesian tensor notation is used throughout.

The exact instantaneous equations for turbulent flow of incompressible FENE-P fluids are:

$$\frac{\partial \widehat{u}_k}{\partial x_k} = 0 \tag{1}$$

$$\rho\left(\frac{\partial \widehat{u}_i}{\partial t} + \widehat{u}_k \frac{\partial \widehat{u}_i}{\partial x_k}\right) = -\frac{\partial \widehat{p}}{\partial x_i} + \frac{\partial \widehat{\tau}_{ik}}{\partial x_k} \tag{2}$$

$$\widehat{\tau}_{ik} = \widehat{\tau}^s_{ik} + \widehat{\tau}^p_{ik} \tag{3}$$

$$\widehat{\tau}^p_{ij} = \frac{\eta_p}{\lambda}\left(f(\widehat{c}_{ij})\widehat{c}_{ij} - f(L)\delta_{ij}\right) \tag{4}$$

$$\frac{\partial \widehat{c}_{ij}}{\partial t} + \widehat{u}_k \frac{\partial \widehat{c}_{ij}}{\partial x_k} - \left(\widehat{c}_{kj}\frac{\partial \widehat{u}_i}{\partial x_k} + \widehat{c}_{ik}\frac{\partial \widehat{u}_j}{\partial x_k}\right) = \overset{\nabla}{\widehat{c}}_{ij} = -\frac{\widehat{\tau}^p_{ij}}{\eta_p} \tag{5}$$

$$f(\widehat{c}_{kk}) = \frac{L^2 - 3}{L^2 - \widehat{c}_{kk}} \text{ and } f(L) = 1 \tag{6}$$

Eq. (1) is the continuity equation, Eq. (2) is the momentum equation in which the total stress is a sum of solvent and polymeric contributions, as defined in Eq. (3). The solvent stress obeys Newton's law of viscosity, the polymeric stress is defined by Eq. (4) and depends on the conformation tensor $\widehat{c}_{ij}$. The evolution equation of $\widehat{c}_{ij}$ is Eq. (5) and the Peterlin function is given in Eq. (6), where L^2 denotes the maximum molecular extensibility and $\widehat{c}_{kk}$ is the trace of the instantaneous conformation tensor.

After applying the Reynolds decomposition [35] (see also [9]) and time-averaging Eqs. (1)–(6), we obtain the so-called Reynolds-averaged Navier–Stokes/Reynolds-averaged conformation evolution (RANS/RACE) equations:

$$\frac{\partial U_i}{\partial x_i} = 0 \tag{7}$$

$$\rho\frac{\partial U_i}{\partial t} + \rho U_k \frac{\partial U_i}{\partial x_k} = -\frac{\partial \bar{p}}{\partial x_i} + \eta_s \frac{\partial^2 U_i}{\partial x_k \partial x_k} - \frac{\partial}{\partial x_k}\left(\rho\overline{u_i u_k}\right) + \frac{\partial \overline{\tau^p_{ik}}}{\partial x_k} \tag{8}$$

In Eqs. (7) and (8) $\bar{p}$ is the mean pressure, U_i is the mean velocity, ρ is the fluid density, $-\rho\overline{u_i u_k}$ is the Reynolds stress tensor and $\overline{\tau^p_{ik}}$ is the Reynolds-averaged polymer stress. In the FENE-P model the time-averaged extra stress is the sum of a Newtonian solvent contribution of viscosity coefficient η_s with a polymeric contribution:

$$\overline{\tau}_{ij} = \eta_s\left(\frac{\partial U_i}{\partial x_j} + \frac{\partial U_j}{\partial x_i}\right) + \overline{\tau}^p_{ij} \tag{9}$$

This Newtonian extra stress has already been incorporated into the momentum Eq. (8). The Reynolds-averaged polymer stress $\overline{\tau}^p_{ij}$ results from Reynolds-averaging the instantaneous FENE-P stress equation (9) and is given by Eq. (10). Then, the average conformation tensor (C_{ij}) is given by the Reynolds average conformation evolution Eq. (11), where the first-term inside the brackets on the left-hand-side is Oldroyd's upper convective derivative of C_{ij}. The various terms have specific designations given below the horizontal brackets.

$$\overline{\tau}^p_{ij} = \frac{\eta_p}{\lambda}\left[f(C_{kk})C_{ij} - f(L)\delta_{ij}\right] + \frac{\eta_p}{\lambda}\overline{f(C_{kk} + c_{kk})c_{ij}} \tag{10}$$

$$\underbrace{\left[\underbrace{\frac{\partial C_{ij}}{\partial t} + U_k\frac{\partial C_{ij}}{\partial x_k}}_{DC_{ij}/Dt} - \underbrace{\left(C_{jk}\frac{\partial U_i}{\partial x_k} + C_{ik}\frac{\partial U_j}{\partial x_k}\right)}_{M_{ij}}\right]}_{} + \underbrace{\overline{u_k\frac{\partial c_{ij}}{\partial x_k}}}_{CT_{ij}} - \underbrace{\left(\overline{c_{kj}\frac{\partial u_i}{\partial x_k}} + \overline{c_{ik}\frac{\partial u_j}{\partial x_k}}\right)}_{NLT_{ij}} = -\frac{\overline{\tau}^p_{ij}}{\eta_p} = T_{ij} \tag{11}$$

The functions appearing in Eq. (10) are those in Eq. (6) and here and henceforth it is important to realise that

$$\overline{f(\widehat{c}_{kk})} = \overline{\frac{L^2 - 3}{L^2 - \widehat{c}_{kk}}} \neq f\left(\overline{\widehat{c}_{kk}}\right) = f(C_{kk}) = \frac{L^2 - 3}{L^2 - C_{kk}} \tag{12}$$

The other parameters of the model are the relaxation time of the polymer λ and its viscosity coefficient η_p. To calculate the molecular conformation and the corresponding polymer stress, it is necessary to quantify the three terms with overbars in Eqs. (10) and (11) using adequate closures.

DNS results are used in this work to guide some of the simplifying assumptions and to calibrate the model coefficients. The DNS data pertain to the low and intermediate drag reduction regimes and are part of extensive data produced by Li et al. [8] and Kim et al. [36,37] for FENE-P fluids in fully-developed turbulent channel flow. The two sets of DNS data used throughout this paper are characterised by the following parameters: a Reynolds number of $Re_{\tau 0} = 395$, a ratio of solvent to total zero-shear-rate viscosities (β) of 0.9 and a maximum extension $L^2 = 900$. The Weissenberg numbers are $We_{\tau 0} = 25$ and $We_{\tau 0} = 100$, corresponding to drag reductions of 18% and 37%, respectively. The non-dimensional numbers are defined as follows: the Reynolds number $Re_{\tau_0} \equiv hu_\tau/\nu_0$ is based on the friction velocity (u_τ), the channel half-height (h) and the zero shear-rate kinematic viscosity of the solution, which is the sum of the kinematic viscosities of the solvent and polymer ($\nu_0 = \nu_s + \nu_p$). The Weissenberg number is given by $We_{\tau_0} \equiv \lambda u_\tau^2/\nu_0$ and the ratio between the solvent viscosity and the solution viscosity at zero shear rate is β ($\beta \equiv \nu_s/\nu_0$).

Housiadas et al. [6] and Li et al. [8] have shown that all terms of $CT_{ij} = -\overline{u_k \partial c_{ij}/\partial x_k}$ are negligible in comparison with the other terms of Eq. (11) at both low and high drag reduction. As a consequence, to close Eq. (11) it is only necessary to develop a closure for the NLT_{ij} term, which accounts for the interactions between the fluctuating components of the conformation and velocity gradient tensors that originate from Oldroyd's upper convected derivative.

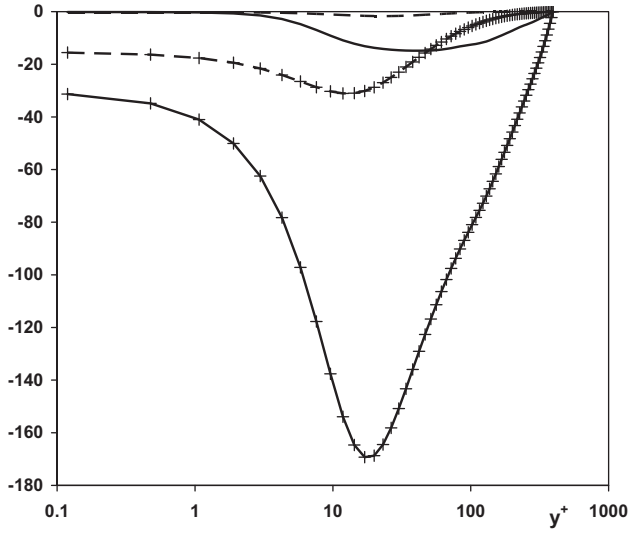

Fig. 1. Comparison between DNS data of $\overline{f(C_{kk}+c_{kk})c_{12}}$ and $f(C_{kk})C_{12}$ for the channel flow of a FENE-P with $Re_\tau = 395$, $L^2 = 900$ and $\beta = 0.9$: (−−) $\overline{f(C_{kk}+c_{kk})c_{12}}$ and (−+−) $f(C_{kk})C_{12}$ for $We_\tau = 25$, DR = 18%; (—) $\overline{f(C_{kk}+c_{kk})c_{12}}$ and (+) $f(C_{kk})C_{12}$ for $We_\tau = 100$, DR = 37%.

Pinho et al. [9] have also demonstrated that it is justifiable to neglect $\overline{f(\widehat{c}_{kk})c_{ij}}$ in Eq. (10), for low drag reduction (LDR). To assess whether that remains valid in the IDR regime, Fig. 1 shows a comparison of the magnitudes of the shear component of $\overline{f(\widehat{c}_{kk})c_{ij}}$ and $f(C_{kk})C_{ij}$ for the two sets of DNS data. At the peak of $\overline{f(\widehat{c}_{kk})c_{ij}}$, the ratio $\overline{f(\widehat{c}_{kk}c_{ij})}/f(C_{kk})C_{ij}$ varies from around 5% at LDR to 20% at IDR. Hence, as a first approximation, this double correlation can still be neglected.

The Reynolds stress tensor in Eq. (8) is modelled by invoking the Boussinesq turbulent stress–strain relationship (13)

$$-\rho\overline{u_i u_j} = 2\rho\nu_T S_{ij} - \frac{2}{3}\rho k\delta_{ij} \tag{13}$$

where k is the turbulent kinetic energy and S_{ij} is the rate of deformation tensor defined in Eq. (14)

$$S_{ij} = \frac{1}{2}\left(\frac{\partial u_i}{\partial x_j} + \frac{\partial u_j}{\partial x_i}\right) \tag{14}$$

In Eq. (13) ν_T is the eddy viscosity, here modelled by a modified form of the Prandtl–Kolmogorov closure, to be explained later. Now, it suffices to say that ν_T is a function of k and the rate of dissipation of k by the Newtonian solvent (ε^N). These two quantities are obtained from their transport equations.

The transport equation for the turbulent kinetic energy is given by Eq. (15), a contraction of the Reynolds stress equation developed by Dimitropoulos et al. [19],

$$\rho\frac{Dk}{Dt} + \rho\overline{u_i u_k}\frac{\partial U_i}{\partial x_k} = -\rho\overline{u_k\frac{\partial k'}{\partial x_k}} - \frac{\partial\overline{pu_i}}{\partial x_i} + \eta_s\frac{\partial^2 k}{\partial x_k^2} - \eta_s\overline{\frac{\partial u_i}{\partial x_k}\frac{\partial u_i}{\partial x_k}} + \frac{\partial}{\partial x_k}\left(\overline{\tau_{ik}^p u_i}\right) - \left(\overline{\tau_{ik}^p\frac{\partial u_i}{\partial x_k}}\right) \tag{15}$$

Introducing the polymeric stress fluctuations into Eq. (15), we obtain the following transport equation for k

$$\rho\frac{Dk}{Dt} = \underbrace{-\rho\overline{u_i u_k}\frac{\partial U_i}{\partial x_k}}_{P_k} \underbrace{-\left(\rho\overline{u_k\frac{\partial k'}{\partial x_k}} + \frac{\partial\overline{pu_i}}{\partial x_i}\right)}_{Q_k} + \underbrace{\eta_s\frac{\partial^2 k}{\partial x_k^2}}_{D_k^N} \underbrace{-\eta_s\overline{\frac{\partial u_i}{\partial x_k}\frac{\partial u_i}{\partial x_k}}}_{\rho\varepsilon^N} + \underbrace{\frac{\eta_p}{\lambda}\frac{\partial}{\partial x_k}\left[C_{ik}\overline{f(C_{mm}+c_{mm})u_i} + \overline{c_{ik}f(C_{mm}+c_{mm})u_i}\right]}_{Q^V} - \underbrace{\frac{\eta_p}{\lambda}\left[C_{ik}\overline{f(C_{mm}+c_{mm})\frac{\partial u_i}{\partial x_k}} + \overline{c_{ik}f(C_{mm}+c_{mm})\frac{\partial u_i}{\partial x_k}}\right]}_{\rho\varepsilon^V} \tag{16}$$

where P_k is the rate of production of k, Q_k is the turbulent transport of k by velocity and pressure fluctuations, D_k^N is the molecular diffusion of k associated with the Newtonian solvent, ε^N is the viscous dissipation of k by the Newtonian solvent, Q^V is the viscoelastic turbulent transport and ε^V is the viscoelastic stress work, which can be positive or negative, acting as a dissipation or production mechanism, respectively. Note that both ε^N and ε^V terms have leading minus signs.

The transport equation for the rate of dissipation of turbulent kinetic energy by the Newtonian solvent was derived by Pinho et al. [9] and is given by:

$$\begin{aligned}\rho\frac{\partial\varepsilon^N}{\partial t} + \rho U_k\frac{\partial\varepsilon^N}{\partial x_k} = &-2\eta_s\left[\frac{\partial U_i}{\partial x_m}\overline{\frac{\partial u_i}{\partial x_m}\frac{\partial u_i}{\partial x_k}} + \frac{\partial U_i}{\partial x_k}\overline{\frac{\partial u_i}{\partial x_m}\frac{\partial u_k}{\partial x_m}}\right]\\ &- 2\eta_s\frac{\partial^2 U_i}{\partial x_m\partial x_k}\overline{u_k\frac{\partial u_i}{\partial x_m}} - 2\eta_s\overline{\frac{\partial u_i}{\partial x_m}\frac{\partial u_i}{\partial x_k}\frac{\partial u_k}{\partial x_m}}\\ &- \frac{\partial}{\partial x_k}\left[\rho\overline{u_k\varepsilon^{N\prime}} + 2\nu_s\overline{\frac{\partial p\prime}{\partial x_m}\frac{\partial u_k}{\partial x_m}}\right] + \eta_s\frac{\partial^2\varepsilon^N}{\partial x_k\partial x_k}\\ &- 2\eta_s\nu_s\overline{\frac{\partial^2 u_i}{\partial x_m\partial x_k}\frac{\partial^2 u_i}{\partial x_m\partial x_k}}\\ &+ 2\nu_s\frac{\eta_p}{\lambda\left(L^2-3\right)}\overline{\frac{\partial u_i}{\partial x_m}\frac{\partial}{\partial x_k}\left\{\frac{\partial}{\partial x_m}\left[f(C_{nn})f(\widehat{c}_{pp})c'_{qq}C_{ik}\right]\right\}}\end{aligned} \tag{17}$$

Except for the last term, the viscoelastic contribution to the transport equation of ε^N, all other terms are identical to those for a Newtonian fluid.

The quantities plotted in all figures are non-dimensionalised using the normalisation of the original DNS data [8]. Specifically, the velocity scale is always taken as the friction velocity, leading to the use of superscript (+) as in $u_i = u_i^+ u_\tau$, but for the spatial coordinates either the channel half-height ($x_i = x_i^* h$) or the viscous length are used ($x_i = x_i^+ \nu_0/u_\tau$), leading to superscripts $*$ and +, respectively. Both normalisations are used in the original DNS data. When mixing the two types of normalisation, i.e., wall/viscous and physical velocity and length scales, the superscript used is $*$, as in $NLT_{ij} = NLT_{ij}^* u_\tau/h$.

3. Closure of the Reynolds average conformation equation

3.1. Exact and approximate equations for NLT_{ij}

An exact expression for NLT_{ij} can be derived as $\overline{L(\widehat{c}_{kj})\frac{\partial u_i}{\partial x_k}\frac{1}{f(\widehat{c}_{mm})}} + \overline{L(\widehat{c}_{ik})\frac{\partial u_j}{\partial x_k}\frac{1}{f(\widehat{c}_{mm})}}$ where the operator $L(\widehat{c}_{kj})$ denotes the instantaneous evolution equation of $\widehat{c}_{kj}$. This is given as Eq. (AI-1) of Appendix I.

An alternative, more compact equation was derived by Pinho [38] as $\overline{L(\widehat{c}_{kj})\frac{\partial u_i}{\partial x_k}} + \overline{L(\widehat{c}_{ik})\frac{\partial u_j}{\partial x_k}}$ given here as:

$$\begin{aligned}\overline{f(\widehat{c}_{mm})c_{kj}\frac{\partial u_i}{\partial x_k}+f(\widehat{c}_{mm})c_{ik}\frac{\partial u_j}{\partial x_k}} &= -\lambda\left[\overline{\frac{\partial u_i}{\partial x_k}\frac{\partial c_{kj}}{\partial t}}+\overline{\frac{\partial u_j}{\partial x_k}\frac{\partial c_{ik}}{\partial t}}\right]\\ &-\left(C_{kj}\overline{f(\widehat{c}_{mm})\frac{\partial u_i}{\partial x_k}}+C_{ik}\overline{f(\widehat{c}_{mm})\frac{\partial u_j}{\partial x_k}}\right)\\ &-\lambda\left[\frac{\partial C_{kj}}{\partial x_n}\overline{u_n\frac{\partial u_i}{\partial x_k}}+\frac{\partial C_{ik}}{\partial x_n}\overline{u_n\frac{\partial u_j}{\partial x_k}}+\overline{\frac{\partial(U_nc_{kj})}{\partial x_n}\frac{\partial u_i}{\partial x_k}}\right.\\ &\left.+\overline{\frac{\partial(U_nc_{ik})}{\partial x_n}\frac{\partial u_j}{\partial x_k}}+\overline{u_n\frac{\partial c_{kj}}{\partial x_n}\frac{\partial u_i}{\partial x_k}}+\overline{u_n\frac{\partial c_{ik}}{\partial x_n}\frac{\partial u_j}{\partial x_k}}\right]\\ &+\lambda\left[\frac{\partial U_k}{\partial x_n}\left(\overline{c_{jn}\frac{\partial u_i}{\partial x_k}}+\overline{c_{in}\frac{\partial u_j}{\partial x_k}}\right)\right.\\ &+\frac{\partial U_j}{\partial x_n}\overline{c_{kn}\frac{\partial u_i}{\partial x_k}}+\frac{\partial U_i}{\partial x_n}\overline{c_{kn}\frac{\partial u_j}{\partial x_k}}\\ &\left.+C_{kn}\left(\overline{\frac{\partial u_j}{\partial x_n}\frac{\partial u_i}{\partial x_k}}+\overline{\frac{\partial u_i}{\partial x_n}\frac{\partial u_j}{\partial x_k}}\right)\right]\\ &+\lambda\left[C_{jn}\overline{\frac{\partial u_k}{\partial x_n}\frac{\partial u_i}{\partial x_k}}+C_{in}\overline{\frac{\partial u_k}{\partial x_n}\frac{\partial u_j}{\partial x_k}}+\overline{c_{jn}\frac{\partial u_k}{\partial x_n}\frac{\partial u_i}{\partial x_k}}\right.\\ &\left.+\overline{c_{in}\frac{\partial u_k}{\partial x_n}\frac{\partial u_j}{\partial x_k}}+\overline{c_{kn}\frac{\partial u_j}{\partial x_n}\frac{\partial u_i}{\partial x_k}}+\overline{c_{kn}\frac{\partial u_i}{\partial x_n}\frac{\partial u_j}{\partial x_k}}\right]\end{aligned} \tag{18}$$

The above expression can be related to NLT_{ij} through the following approximation:

$$\begin{aligned}\overline{f(\widehat{c}_{mm})c_{kj}\frac{\partial u_i}{\partial x_k}}+\overline{f(\widehat{c}_{mm})c_{ik}\frac{\partial u_j}{\partial x_k}} &\approx f(C_{mm})\left(\overline{c_{kj}\frac{\partial u_i}{\partial x_k}}+\overline{c_{ik}\frac{\partial u_j}{\partial x_k}}\right)\\ &= f(C_{mm})NLT_{ij}\end{aligned} \tag{19}$$

The above approximation is justified by comparing DNS data for the exact and approximate functions: see Fig. 2(a) (LDR) and (b) (IDR). In both regimes the triple correlation and the corresponding approximation have the same form, an indication that the latter captures the features of the former and that only a coefficient of proportionality is required. Near the wall, there is always a good match between the triple correlation and $f(C_{mm})\times NLT_{ij}$ and a difference is shown essentially to occur in the region of the positive peak, which increases with Weissenberg number. Hence, $f(C_{mm})NLT_{ij}$ will be quantified by the r.h.s. of Eq. (18), which needs modelling, multiplied by such coefficient of proportionality. The essential feature of the model is to capture this Weissenberg number dependence away from the wall, and because NLT_{ij} is not that important close to the wall any discrepancy in the near wall region will be of little consequence to the turbulence model predictions.

The approximation of Eq. (19) can also be understood by analysing the comparison between the time-averaged trace of the conformation tensor (C_{kk}) and its r.m.s. ($\sqrt{\overline{c_{kk}^2}}$) plotted in Fig. 3 for DR = 18% and 37%. Near the walls the molecules are more stretched and the traces of the conformation tensor are larger, so $f(\widehat{c}_{kk})$ is different from its equilibrium value of 1 (not shown for conciseness), $\sqrt{\overline{c_{kk}^2}} \ll C_{kk}$ and $\sqrt{\overline{c_{kk}^2}}/C_{kk}$ decreases with drag reduction varying from 23% at DR = 18% to 10% for DR = 37%. Thus, here it is justifiable to neglect the r.m.s. in comparison with the time-averaged value with all its implications regarding function $f(\widehat{c}_{kk})$. At the centreline $\sqrt{\overline{c_{kk}^2}}$ approaches C_{kk}, but both quantities decrease to small values and consequently $f(\widehat{c}_{kk}) \approx f(C_{kk}) \approx 1$ (for $C_{kk}=50$ and 100, $f(C_{kk})=1.06$ and 1.12, respectively). This justifies neglecting $\sqrt{\overline{c_{kk}^2}}$ in comparison with C_{kk} when calculating $f(C_{kk})$, as found previously for LDR [9]. At IDR the molecules are more stretched, the difference in magnitudes of $\sqrt{\overline{c_{kk}^2}}$ and C_{kk} actually increases and on the centreline region $\sqrt{\overline{c_{kk}^2}}$ is now lower than C_{kk}.

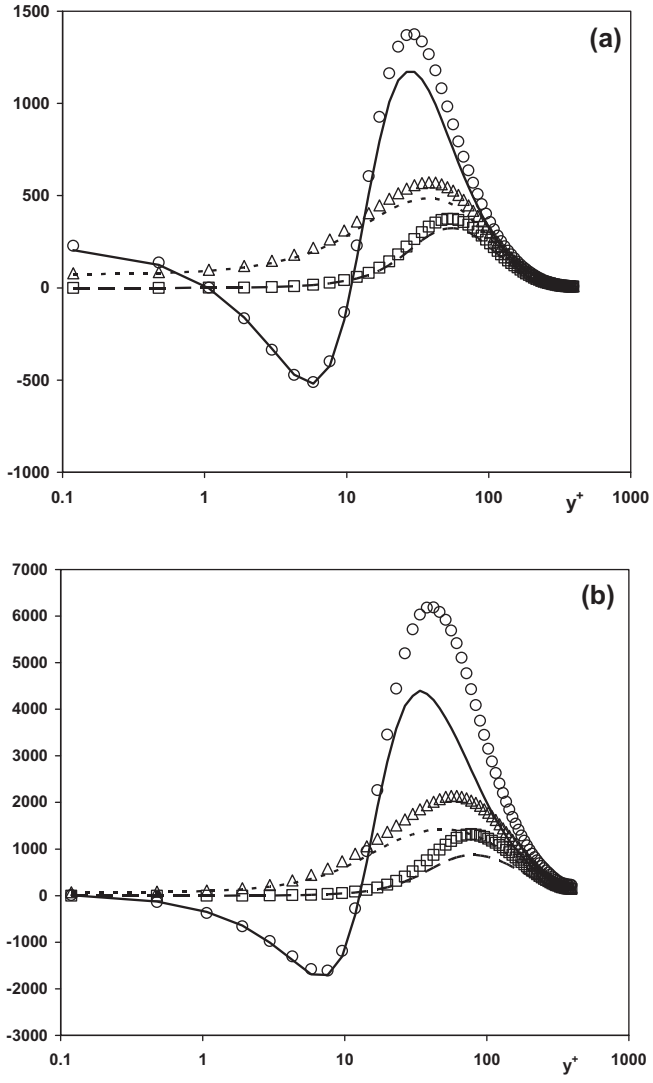

Fig. 2. Comparison between components of $\overline{f(\widehat{c}_{mm})c_{kj}\frac{\partial u_i}{\partial x_k}^{*}+f(\widehat{c}_{mm})c_{ik}\frac{\partial u_j}{\partial x_k}^{*}}$ (symbols) and of $f(C_{mm})NLT_{ij}^{*}$ (lines) for channel flow of FENE-P fluids at $Re_\tau=395$, $L^2=900$ and $\beta=0.9$: (a)$We_\tau=25$, DR = 18%; (b)$We_\tau=100$, DR = 37%: (○) $2\overline{fc\prime_{1k}\partial u_{1}\prime/\partial x_k^{*}}$; (△) $2\overline{fc\prime_{3k}\partial u_{3}\prime/\partial x_k^{*}}$; (□) $2\overline{fc\prime_{2k}\partial u_{2}\prime/\partial x_k^{*}}$; (—) $f(C_{kk})NLT_{11}^{*}$; (– –) $f(C_{kk})NLT_{22}^{*}$; (– – –) $f(C_{kk})NLT_{33}^{*}$.

Given the form of function $f(\widehat{c}_{kk})$ the fluctuations c_{kk} have a small influence on the triple correlation in Eq. (19) and the function $f(\widehat{c}_{kk})$ can come out of the time-average. Another implication of $\sqrt{\overline{c_{kk}^2}} \ll C_{kk}$ is that it is also justifiable to consider $\overline{f(\widehat{c}_{kk})} \approx f(C_{kk})$. Both these relations will be used to derive closures.

3.2. Development of a model for NLT_{ij}

Equating the r.h.s. of Eq. (18) to $f(C_{mm})\,NLT_{ij}$ and solving in order to NLT_{ij} provides an equation for NLT_{ij} that needs to be modelled. On the basis of DNS data analysis some terms of such equation will be neglected with physical insight and theoretical considerations providing the arguments for the closure of the remaining terms. This will require certain assumptions to be made with their validity checked later once DNS data for higher and maximum drag reductions become available. The assumptions that were adopted here were as follows:

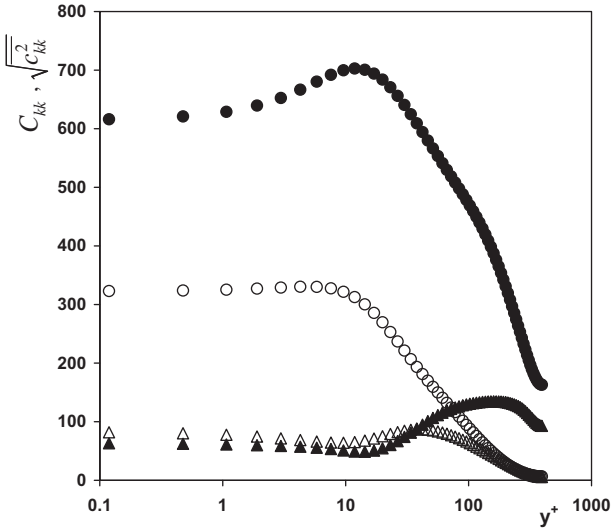

Fig. 3. Transverse profiles of C_{kk} (○) and $\sqrt{\overline{c_{kk}^2}}$ (△) for channel flow of FENE-P fluids with $Re_\tau = 395$, $L^2 = 900$ and $\beta = 0.9$: (open symbols) $We_\tau = 25$, DR = 18%; (close symbols) $We_\tau = 100$, DR = 37%.

(1) All cross-correlations between velocity fluctuations and gradients of the fluctuating conformation tensor ($\overline{u_n(\partial c_{ij}/\partial x_k)}$) are negligible, regardless of the indices. This is correct for CT_{ij} [5,6], but needs to be demonstrated for other index combinations.

(2) Turbulence is homogeneous away from solid walls leading to the neglect of contributions having similarities with turbulent diffusion of turbulent kinetic energy. This requires confirmation for polymer flows, at least for some combinations of indices. For Newtonian fluids it is a reasonable assumption except near walls. This assumption implies that

$$\overline{u_n \frac{\partial u_j}{\partial x_k}} = 0 \tag{20}$$

(3) Invariance requires that convective terms are null except as part of a material derivative which is not the case here. Hence,

$$U_n\left(\overline{\frac{\partial c_{kj}}{\partial x_n}\frac{\partial u_i}{\partial x_k}} + \overline{\frac{\partial c_{ik}}{\partial x_n}\frac{\partial u_j}{\partial x_k}}\right) + \overline{u_n\frac{\partial c_{kj}}{\partial x_n}\frac{\partial u_i}{\partial x_k}} + \overline{u_n\frac{\partial c_{ik}}{\partial x_n}\frac{\partial u_j}{\partial x_k}} \approx 0 \tag{21}$$

Based on these three assumptions the NLT_{ij} expression simplifies to Eq. (22), which still contains terms that need to be modelled.

$$\begin{aligned} NLT_{ij} \approx & -\frac{1}{f(C_{mm})}\left(C_{kj}\overline{f(\hat{c}_{mm})\frac{\partial u_i}{\partial x_k}} + C_{ik}\overline{f(\hat{c}_{mm})\frac{\partial u_j}{\partial x_k}}\right) \\ & + \frac{\lambda}{f(C_{mm})}\left[\frac{\partial U_k}{\partial x_n}\left(\overline{c_{jn}\frac{\partial u_i}{\partial x_k}} + \overline{c_{in}\frac{\partial u_j}{\partial x_k}}\right) + \frac{\partial U_j}{\partial x_n}\overline{c_{kn}\frac{\partial u_i}{\partial x_k}}\right. \\ & \left. + \frac{\partial U_i}{\partial x_n}\overline{c_{kn}\frac{\partial u_j}{\partial x_k}} + C_{kn}\left(\overline{\frac{\partial u_j}{\partial x_n}\frac{\partial u_i}{\partial x_k}} + \overline{\frac{\partial u_i}{\partial x_n}\frac{\partial u_j}{\partial x_k}}\right)\right] \\ & + \frac{\lambda}{f(C_{mm})}\left[C_{jn}\overline{\frac{\partial u_k}{\partial x_n}\frac{\partial u_i}{\partial x_k}} + C_{in}\overline{\frac{\partial u_k}{\partial x_n}\frac{\partial u_j}{\partial x_k}} + \overline{c_{jn}\frac{\partial u_k}{\partial x_n}\frac{\partial u_i}{\partial x_k}}\right. \\ & \left. + \overline{c_{in}\frac{\partial u_k}{\partial x_n}\frac{\partial u_j}{\partial x_k}} + \overline{c_{kn}\frac{\partial u_j}{\partial x_n}\frac{\partial u_i}{\partial x_k}} + \overline{c_{kn}\frac{\partial u_i}{\partial x_n}\frac{\partial u_j}{\partial x_k}}\right] \end{aligned} \tag{22}$$

3.2.1. Closure for the double correlations between fluctuating strain rates

To model Eq. (22) we start with the four terms involving the cross-correlations between two fluctuating rates of strain on its r.h.s., which are

$$C_{kn}\left(\overline{\frac{\partial u_j}{\partial x_n}\frac{\partial u_i}{\partial x_k}} + \overline{\frac{\partial u_i}{\partial x_n}\frac{\partial u_j}{\partial x_k}}\right) + C_{jn}\overline{\frac{\partial u_k}{\partial x_n}\frac{\partial u_i}{\partial x_k}} + C_{in}\overline{\frac{\partial u_k}{\partial x_n}\frac{\partial u_j}{\partial x_k}} \tag{23}$$

The relation between the double correlation of fluctuating strain rates and the turbulence kinetic energy in homogeneous isotropic turbulence is given by Eq. (24) [39], where λ_f is Taylor's longitudinal micro-scale. This length scale is associated with streamwise gradients of fluctuating streamwise quantities, whereas for the gradients of cross-stream quantities Taylor's transversal length scale (λ_g) is used, but both are related by $\lambda_g^2 = \lambda_f^2/2$.

$$\overline{\frac{\partial u_i}{\partial x_k}\frac{\partial u_j}{\partial x_l}} = \frac{8}{3}\frac{k}{\lambda_f^2}\left[\delta_{ij}\delta_{kl} - \frac{1}{4}\left(\delta_{ik}\delta_{jl} + \delta_{il}\delta_{jk}\right)\right] \tag{24}$$

In homogeneous isotropic turbulence Eq. (24) has the following four possible outcomes:

$$(1)\ \text{when } i=j=k=l,\ \overline{\frac{\partial u_i}{\partial x_k}\frac{\partial u_j}{\partial x_l}} = \frac{4}{3}\frac{k}{\lambda_f^2} \tag{25a}$$

$$(2)\ \text{when } i=j \text{ and } k=l,\ \text{with } i\neq k,\ \overline{\frac{\partial u_i}{\partial x_k}\frac{\partial u_j}{\partial x_l}} = \frac{8}{3}\frac{k}{\lambda_f^2} \tag{25b}$$

$$(3)\ \text{when } i=l \text{ and } k=j,\ \text{with } i\neq k,\ \overline{\frac{\partial u_i}{\partial x_k}\frac{\partial u_j}{\partial x_l}} = -\frac{2}{3}\frac{k}{\lambda_f^2} \tag{25c}$$

$$(4)\ \text{zero otherwise} \tag{25d}$$

At high Reynolds number homogeneous isotropic turbulence, Taylor's longitudinal micro-scale is related to the dissipation of turbulent kinetic energy via Eq. (26). Here, we consider that this dissipation is that by the Newtonian solvent (ε^N).

$$\varepsilon^N = 20\frac{\nu_s k}{\lambda_f^2} \tag{26}$$

Hence, those four terms are modelled as

$$\begin{aligned} & C_{kn}\left(\overline{\frac{\partial u_j}{\partial x_n}\frac{\partial u_i}{\partial x_k}} + \overline{\frac{\partial u_i}{\partial x_n}\frac{\partial u_j}{\partial x_k}}\right) + C_{jn}\overline{\frac{\partial u_k}{\partial x_n}\frac{\partial u_i}{\partial x_k}} + C_{in}\overline{\frac{\partial u_k}{\partial x_n}\frac{\partial u_j}{\partial x_k}} \\ & \quad \approx \frac{4}{15}\times\frac{\varepsilon^N}{\nu_s}\times C_{mm}\times\delta_{ij} \end{aligned} \tag{27}$$

which brings the rate of dissipation of k by the Newtonian solvent to contribute to NLT_{ij}.

The model of Eq. (27) is isotropic, whereas DNS shows NLT_{ij} to be anisotropic. Since the model of NLT_{ij} is made of closures for the various terms in Eq. (22) the assessment of its performance requires improvements in several of its components. Essentially, the main contribution of Eq. (27) to the full NLT_{ij} model is in the prediction of its yy and zz components. The anisotropic NLT_{ij} behaves very much like the Newtonian rate of dissipation tensor, ε_{ij}^N, and this has implications on modelling. If the model for NLT_{ij} is to be used in the context of a second order turbulence closure, then ε_{ij}^N is available and can be used to provide the anisotropy in NLT_{ij}. This leads to an alternative proposal for the closure of term (27) given as Eq. (28), where we invoke an argument of isotropy in reverse, i.e., that $\varepsilon_{ij}^N = \frac{2}{3}\varepsilon^N\delta_{ij} \rightarrow \varepsilon^N\delta_{ij} = \frac{3}{2}\varepsilon_{ij}^N$

$$\begin{aligned} & C_{kn}\left(\overline{\frac{\partial u_j}{\partial x_n}\frac{\partial u_i}{\partial x_k}} + \overline{\frac{\partial u_i}{\partial x_n}\frac{\partial u_j}{\partial x_k}}\right) + C_{jn}\overline{\frac{\partial u_k}{\partial x_n}\frac{\partial u_i}{\partial x_k}} + C_{in}\overline{\frac{\partial u_k}{\partial x_n}\frac{\partial u_j}{\partial x_k}} \\ & \quad \approx \frac{2}{5}\times\frac{\varepsilon_{ij}^N}{\nu_s}\times C_{mm} \end{aligned} \tag{28}$$

By using ε_{ij}^N in Eq. (28) the significant anisotropy in NLT_{ij} is captured, but there is also a deficit in predicting NLT_{12}, which increases with drag reduction, as shown in Fig. 4. This figure compares the DNS for NLT_{12} with the prediction of this quantity by the full closure using the contribution of Eq. (28) for the cross-correlation between fluctuating strain rates. Obviously, this only makes sense in the context of second order turbulence models, where ε_{ij}^N is calculated without invoking isotropy arguments.

If the model for NLT_{ij} is to be used in the context of first order turbulence closures, like k–ε or k–ω, ε_{ij}^N is calculated assuming that $\varepsilon_{ij}^N = \frac{2}{3}\varepsilon^N\delta_{ij}$, hence Eq. (28) becomes Eq. (26), hence to provide anisotropy to the full closure of NLT_{ij} via this contribution a different approach is used, as described next.

The contribution of Eq. (27) was calibrated essentially considering the NLT_{22} component, i.e., by using the DNS profile of ε_{22}^N and $\varepsilon^N = \frac{3}{2}\varepsilon_{22}^N$. This component of NLT_{ij} is the most important to predict a correct evolution of the conformation tensor close to the wall, very much as with the corresponding component of the Reynolds stress tensor in second order turbulence models. However, this procedure generates a deficit in the predictions of NLT_{33} and the definition of Eq. (27) leads to a null contribution to NLT_{12}, whereas that is not true as observed in the DNS plots of Figs. 4 and 5, the latter plotting profiles of ε_{22}^N and ε_{12}^N. NLT_{12} is non-zero and as will be shown later in Fig. 10, its peak value is of the order of the peak value of NLT_{22}. To correct the predictions for the shear component of NLT_{ij}, the extra term on the shear rate tensor and its invariant was introduced into the model of Eq. (27) leading to the final form of the closure for this contribution as in Eq. (29). The impact of this modification is clear in Fig. 6 comparing the predictions of NLT_{ij} with and without this correction.

$$C_{kn}\left(\overline{\frac{\partial u_j}{\partial x_n}\frac{\partial u_i}{\partial x_k}}+\overline{\frac{\partial u_i}{\partial x_n}\frac{\partial u_j}{\partial x_k}}\right)+C_{jn}\overline{\frac{\partial u_k}{\partial x_n}\frac{\partial u_i}{\partial x_k}}+C_{in}\overline{\frac{\partial u_k}{\partial x_n}\frac{\partial u_j}{\partial x_k}}$$
$$\approx C_{\varepsilon_F}f_{F2}\left(\frac{25}{We_{\tau 0}}\right)^{0.88}\frac{4}{15}\frac{\varepsilon^N C_{mm}}{\beta v_s}\left(\delta_{ij}+\frac{S_{ij}}{\sqrt{2S_{pq}S_{pq}}}\right) \quad (29)$$

Parameter C_{ε_F} was introduced to account for modelling simplifications, the damping function f_{F2} takes care of low Reynolds number effects near the wall and the ratio with the Weissenberg number

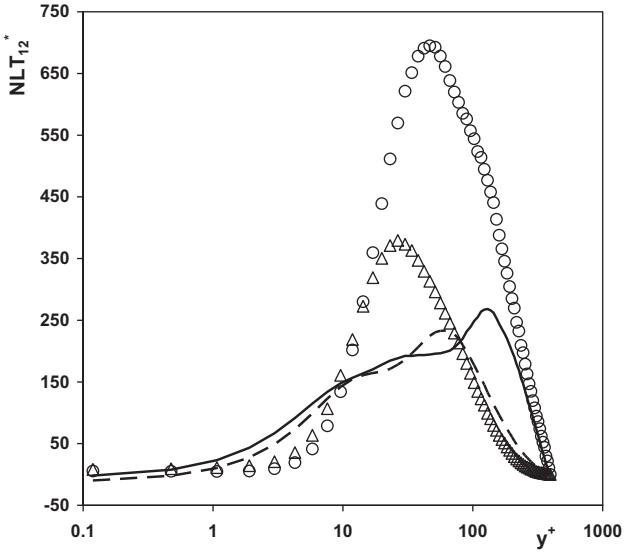

Fig. 4. Transverse profiles of DNS data for NLT_{12}^* (△, $We_{\tau 0}$ = 25, DR = 18% and ○, $We_{\tau 0}$ = 100, DR = 37%); and the NLT_{12}^* general model (– –, $We_{\tau 0}$ = 25, DR = 18% and —, $We_{\tau 0}$ = 100, DR = 37%) with anisotropic effect through the dissipation tensor, ε_{ij}^N, in channel flow of FENE-P fluids with Re_τ = 395, L^2 = 900, β = 0.9.

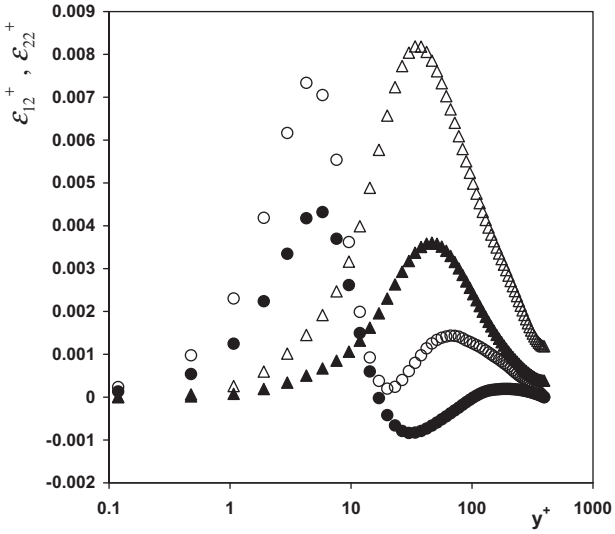

Fig. 5. Transverse profiles of DNS data for ε_{12}^+ (○) and ε_{22}^+ (△) in channel flow of FENE-P fluids with Re_τ = 395, L^2 = 900, β = 0.9: (open symbols) $We_{\tau 0}$ = 25, DR = 18% and (close symbols) $We_{\tau 0}$ = 100, DR = 37%.

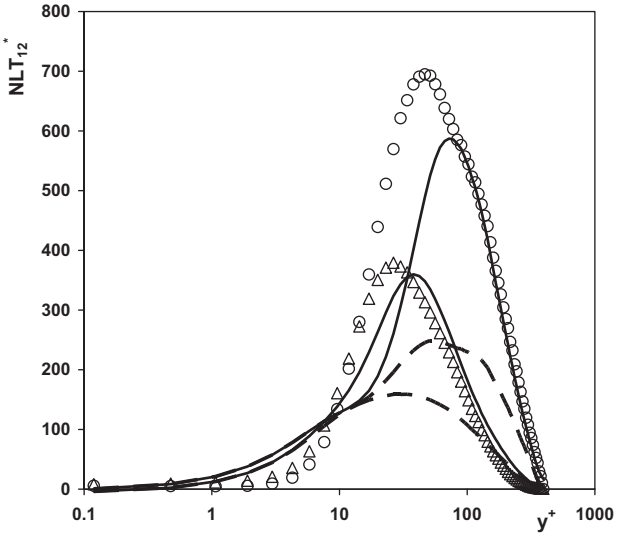

Fig. 6. Transverse profiles of DNS data for NLT_{12}^* (○); and the NLT_{12}^* model without (– –, $We_{\tau 0}$ = 100, DR = 37% and - - -, $We_{\tau 0}$ = 25, DR = 18%) and with (—) anisotropic effect (S_{ij} extra term in Eq. (29)) in channel flow of FENE-P fluids with Re_τ = 395, L^2 = 900, β = 0.9: (Δ)$We_{\tau 0}$ = 25, DR = 18% and (○)$We_{\tau 0}$ = 100, DR = 37%.

$\left(\frac{25}{We_{\tau 0}}\right)^{0.88}$ accounts for the faster increase in the triple correlation seen above in Fig. 2. The quantification of C_{ε_F} and the specific form of f_{F2} were obtained using DNS data at the same time as for the coefficients and functions for the other contributions in order to construct the best possible model for NLT_{ij}. All functions and the numerical values of all coefficients are listed in Section 3.2.5, after Eq. (35).

3.2.2. Closure for the double correlation with $f(\hat{c}_{mm})$

Invoking the previously adopted assumptions, especially regarding $f(\hat{c}_{mm})$ at the end of Section 3.1, the model for the terms containing $\overline{f(\hat{c}_{mm})\frac{\partial u_i}{\partial x_k}}$ and $\overline{f(\hat{c}_{mm})\frac{\partial u_j}{\partial x_k}}$ in Eq. (22) should be zero, since $C_{kj}\overline{f(\hat{c}_{mm})\frac{\partial u_i}{\partial x_k}} \approx C_{kj}f(C_{mm})\overline{\frac{\partial u_i}{\partial x_k}} = 0$.

However, there are advantages in modelling this term as in Eq. (30), where all fluctuating quantities are simply substituted by the corresponding time-averaged quantities (a decoupling of the double correlation into the corresponding individual time-average terms).

$$C_{kj}\overline{f(\widehat{c}_{mm})\frac{\partial u_i}{\partial x_k}} + C_{ik}\overline{f(\widehat{c}_{mm})\frac{\partial u_j}{\partial x_k}} \approx C_{F2}\left[C_{kj}f(C_{mm})\frac{\partial U_i}{\partial x_k} + C_{ik}f(C_{mm})\frac{\partial U_j}{\partial x_k}\right] \tag{30}$$

This is equivalent to a near wall region model, where velocity fluctuations are of the order of the mean velocity. Not surprisingly, it is also here that the mean velocity gradient, mean conformation tensor and function $f(C_{mm})$ reach their maxima and where this modelled term is important. We designate the closure of Eq. (30) as the C_{F2} term and its contribution to the NLT_{ij} model is assessed in Fig. 7, which also shows the full NLT_{ij} model with and without this contribution. In fully-developed channel flow this term only contributes to the NLT_{11} component.

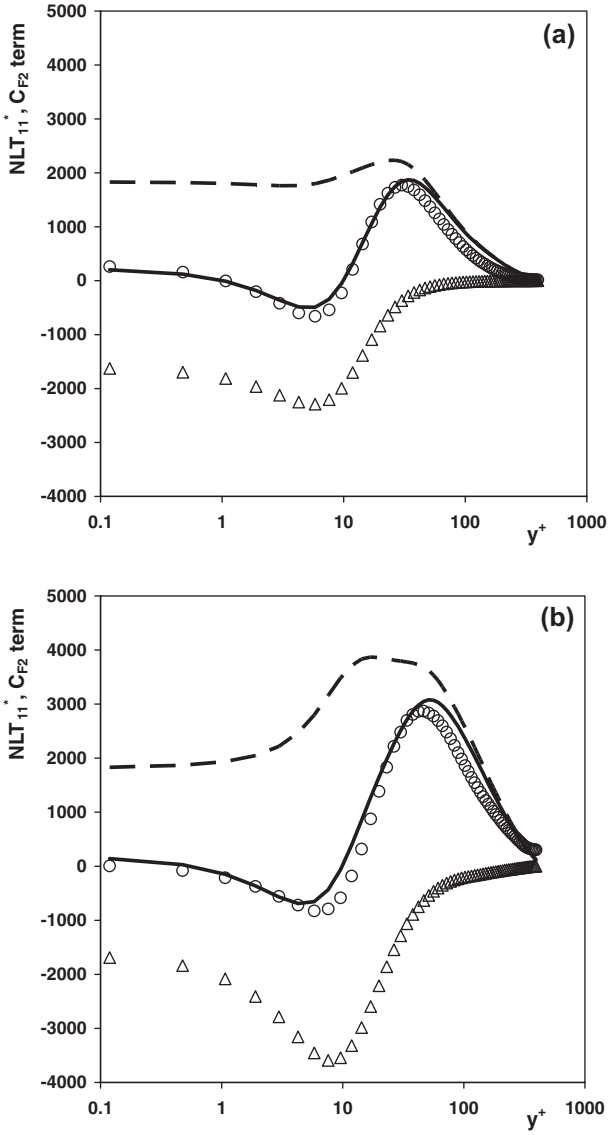

Fig. 7. Transverse profiles of DNS data for NLT^*_{11} (○), C_{F2} term (△), and NLT^*_{11} model without (−−) and with (—) the C_{F2} contribution in channel flow of FENE-P fluids with $Re_\tau = 395$, $L^2 = 900$, $\beta = 0.9$: (a) $We_{\tau 0} = 25$, DR = 18% and (b) $We_{\tau 0} = 100$, DR = 37%.

3.2.3. Closure for the triple correlation

To deal with the four triple correlations of Eq. (22) we followed on the steps of classical turbulence modelling and constitutive equation modelling, where to a first approximation an n^{th}-order correlation can be decoupled into the product of lower order correlations as invoked above. For the model in Eq. (31) all fluctuating quantities were transformed into their corresponding time-averaged quantities and the damping function f_{F1} was used to account for low Reynolds number effects.

$$\begin{aligned}&\overline{c_{jn}\frac{\partial u_k}{\partial x_n}\frac{\partial u_i}{\partial x_k}} + \overline{c_{in}\frac{\partial u_k}{\partial x_n}\frac{\partial u_j}{\partial x_k}} + \overline{c_{kn}\frac{\partial u_j}{\partial x_n}\frac{\partial u_i}{\partial x_k}} + \overline{c_{kn}\frac{\partial u_i}{\partial x_n}\frac{\partial u_j}{\partial x_k}}\\ &\quad\approx -f_{F1}\times\frac{C_{F4}}{We_{\tau 0}}\times\left[C_{jn}\frac{\partial U_k}{\partial x_n}\frac{\partial U_i}{\partial x_k} + C_{in}\frac{\partial U_k}{\partial x_n}\frac{\partial U_j}{\partial x_k}\right.\\ &\quad\left.+ C_{kn}\frac{\partial U_j}{\partial x_n}\frac{\partial U_i}{\partial x_k} + C_{kn}\frac{\partial U_i}{\partial x_n}\frac{\partial U_j}{\partial x_k}\right]\end{aligned} \tag{31}$$

An alternative closure, based on a decoupling of the third order correlation into the product of the time-averaged conformation tensor with the double correlation of the fluctuating rates of deformation, would lead to a contribution identical to that of Eq. (23). This contribution, designated as the C_{F_4} term, corrects the behaviour of NLT_{ij} in the buffer and inner log-layers and its impact is higher at LDR as shown in Fig. 8, where the DNS data is compared with the NLT_{ij} closure without and with this contribution.

3.2.4. Closure for the cross-correlation between fluctuating strain rate and conformation tensors

Modelling the contribution to Eq. (22) presented in Eq. (32) was more difficult and required an *ad-hoc* approach based on physical arguments.

$$\frac{\partial U_k}{\partial x_n}\left(\overline{c_{jn}\frac{\partial u_i}{\partial x_k}} + \overline{c_{in}\frac{\partial u_j}{\partial x_k}}\right) + \frac{\partial U_j}{\partial x_n}\overline{c_{kn}\frac{\partial u_i}{\partial x_k}} + \frac{\partial U_i}{\partial x_n}\overline{c_{kn}\frac{\partial u_j}{\partial x_k}} \tag{32}$$

First, the cross-correlation was decoupled as in Eq. (33), introducing a mixed viscous and turbulent length scale, $L \approx \nu_0/\sqrt{\overline{u_i u_m}}$, aimed at capturing anisotropy effects near the wall. It was convenient to use the Reynolds shear stress when modelling normal components of NLT_{ij}, so the model of Eq. (34) required the inclusion of further quantities for tensorial consistency and the compliance with symmetry and invariance properties of the original term.

$$\frac{\partial U_j}{\partial x_n}\overline{c_{kn}\frac{\partial u_i}{\partial x_k}} \sim \frac{\partial U_j}{\partial x_n}C_{kn}\frac{\sqrt{\overline{u_i u_m}}}{L} \tag{33}$$

$$\begin{aligned}&\frac{\partial U_k}{\partial x_n}\left(\overline{c_{jn}\frac{\partial u_i}{\partial x_k}} + \overline{c_{in}\frac{\partial u_j}{\partial x_k}}\right) + \frac{\partial U_j}{\partial x_n}\overline{c_{kn}\frac{\partial u_i}{\partial x_k}} + \frac{\partial U_i}{\partial x_n}\overline{c_{kn}\frac{\partial u_j}{\partial x_k}}\\ &\quad\approx \frac{C_{F3}}{C_{mm}}\times\left[\frac{\partial U_j}{\partial x_n}\frac{\partial U_m}{\partial x_k}C_{kn}\frac{\overline{u_i u_m}}{\nu_0\sqrt{2S_{pq}S_{pq}}} + \frac{\partial U_i}{\partial x_n}\frac{\partial U_m}{\partial x_k}C_{kn}\frac{\overline{u_j u_m}}{\nu_0\sqrt{2S_{pq}S_{pq}}}\right.\\ &\quad\left.+\frac{\partial U_k}{\partial x_n}\frac{\partial U_m}{\partial x_k}\left(C_{jn}\frac{\overline{u_i u_m}}{\nu_0\sqrt{2S_{pq}S_{pq}}} + C_{in}\frac{\overline{u_j u_m}}{\nu_0\sqrt{2S_{pq}S_{pq}}}\right)\right]\end{aligned} \tag{34}$$

Since the degree of anisotropy of the Reynolds stress tensor was stronger than that of NLT_{ij} near the wall, it had to be reduced and this was achieved by the introduction of the trace of the conformation tensor in the denominator instead of the use of a damping function. Parameter C_{F3} takes the numerical value listed in Table 1.

3.2.5. Buffer layer corrections and the full NLT_{ij} model for second order turbulence closures

To correct the deficiency in predicting NLT_{11} in the viscous and buffer layers there was the need to add an extra term to the closure for NLT_{ij}, as can be seen in Fig. 9. The added term, designated as the C_{F1} term, is the first on the r.h.s. of Eq. (35), which presents the full model of NLT_{ij} for second order turbulence closures.

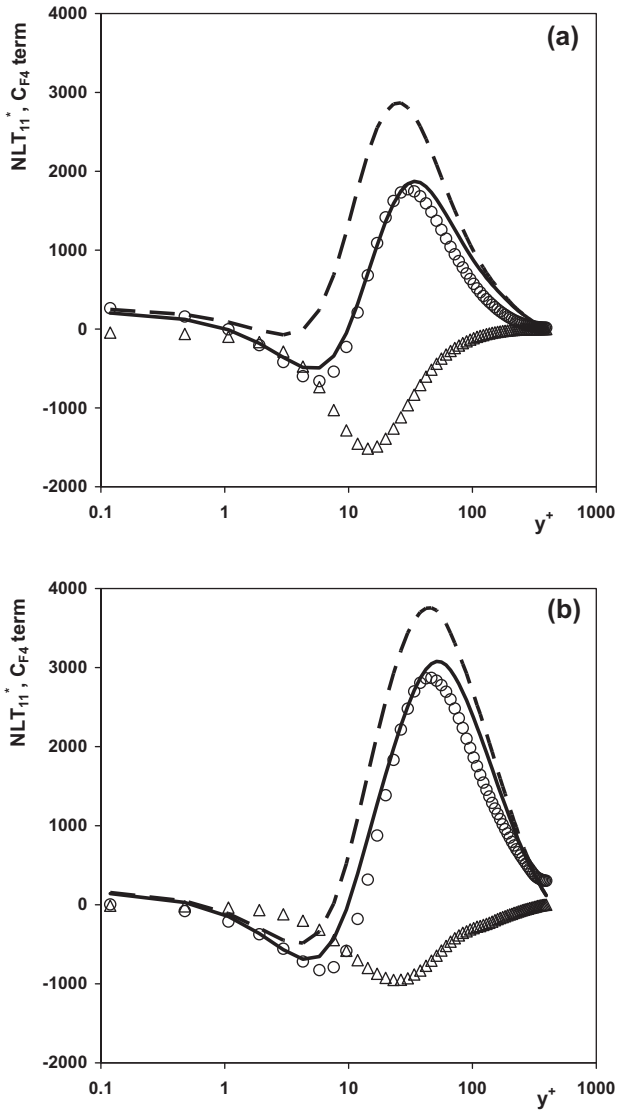

Fig. 8. Transverse profiles of DNS data for NLT_{11}^{*} (○), C_{F4} term (△), and NLT_{11}^{*} model without (−−) and with (—) the C_{F4} term in channel flow of FENE-P fluids with $Re_\tau = 395$, $L^2 = 900$, $\beta = 0.9$: (a)$We_{\tau 0} = 25$, DR = 18% and (b) $We_{\tau 0} = 100$, DR = 37%.

$$
\begin{aligned}
NLT_{ij} &\equiv \overline{c_{kj}\frac{\partial u_i}{\partial x_k}} + \overline{c_{ik}\frac{\partial u_j}{\partial x_k}} \\
&\approx C_{F1} \times \frac{C_{ij} \times f(C_{mm})}{\lambda} - C_{F2}\left[C_{kj}\frac{\partial U_i}{\partial x_k} + C_{ik}\frac{\partial U_j}{\partial x_k}\right] \\
&\quad + \frac{\lambda}{f(C_{mm})}\left[\frac{C_{F3}}{C_{mm}} \times \left(\frac{\partial U_j}{\partial x_n}\frac{\partial U_m}{\partial x_k} C_{kn}\frac{\overline{u_i u_m}}{v_0\sqrt{2S_{pq}S_{pq}}}\right.\right. \\
&\quad + \frac{\partial U_i}{\partial x_n}\frac{\partial U_m}{\partial x_k} C_{kn}\frac{\overline{u_j u_m}}{v_0\sqrt{2S_{pq}S_{pq}}} \\
&\quad \left.\left. + \frac{\partial U_k}{\partial x_n}\frac{\partial U_m}{\partial x_k}\left(C_{jn}\frac{\overline{u_i u_m}}{v_0\sqrt{2S_{pq}S_{pq}}} + C_{in}\frac{\overline{u_j u_m}}{v_0\sqrt{2S_{pq}S_{pq}}}\right)\right)\right] \\
&\quad - \frac{\lambda}{f(C_{mm})} \times f_{F1} \times \frac{C_{F4}}{We_{\tau 0}} \times \left[C_{jn}\frac{\partial U_k}{\partial x_n}\frac{\partial U_i}{\partial x_k} + C_{in}\frac{\partial U_k}{\partial x_n}\frac{\partial U_j}{\partial x_k}\right. \\
&\quad \left. + C_{kn}\frac{\partial U_j}{\partial x_n}\frac{\partial U_i}{\partial x_k} + C_{kn}\frac{\partial U_i}{\partial x_n}\frac{\partial U_j}{\partial x_k}\right] + \frac{\lambda}{f(C_{mm})}\left(\frac{25}{We_{\tau 0}}\right)^{0.88} \\
&\quad \times \left[C_{\varepsilon_F}\frac{4}{15} \times \frac{\varepsilon^N}{v_s \times \beta} C_{mm} \times f_{F2} \times \left(\delta_{ij} + \frac{S_{ij}}{\sqrt{2S_{pq}S_{pq}}}\right)\right] \qquad (35)
\end{aligned}
$$

Table 1
Values of the model parameters for the isotropic NLT_{ij} model.

C_{F1}	C_{F2}	C_{F3}	C_{F4}	C_{ε_F}
1	0.0105	0.046	1.05	2

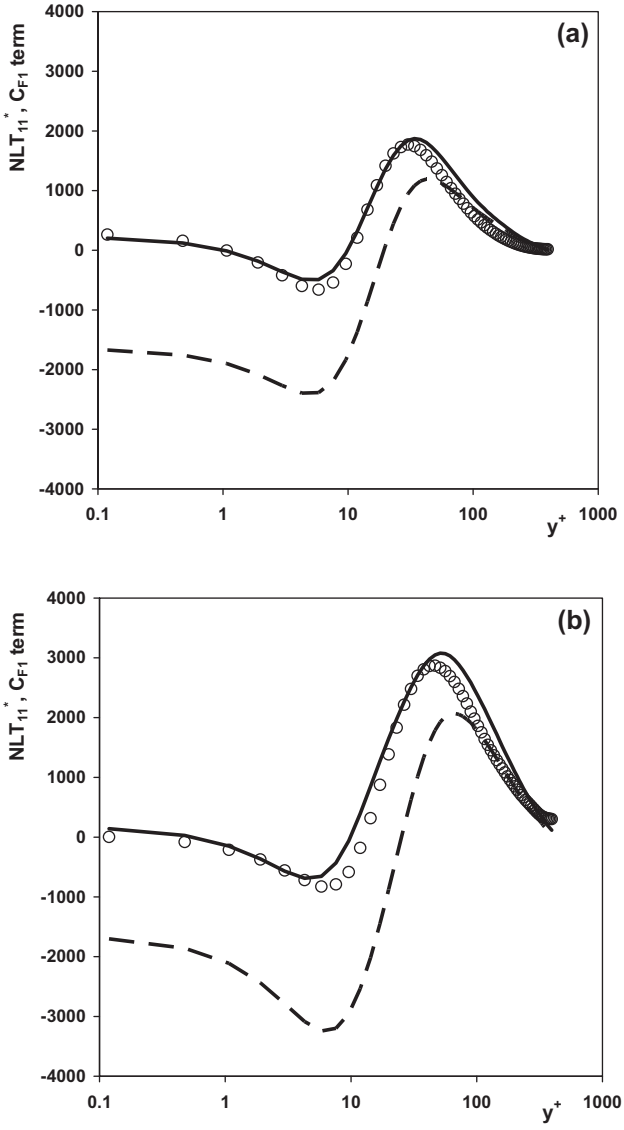

Fig. 9. Axial profile of DNS data for NLT_{11}^{*} (○) and NLT_{11}^{*} model without (−−) and with (—) the C_{F1} term for the channel flow of FENE-P fluids with $Re_\tau = 395$, $L^2 = 900$, $\beta = 0.9$: (a) $We_{\tau 0} = 25$, DR = 18% and (b) $We_{\tau 0} = 100$, DR = 37%.

The numerical values of the coefficients obtained during the calibration are: $C_{F1} = 0.24$, $C_{F2} = 0.2$, $C_{F3} = 2$, $C_{F4} = 10$ and $C_{\varepsilon_F} = 0.049$.

The two damping functions required to capture the near wall behaviour vary, as usual for Newtonian fluids, from zero at the wall to one far from the wall and are given by Eqs. (36) and (37).

$$f_{F1} = \left(1 - 0.67\exp\left(-\frac{y^+}{17}\right)\right)^4 \qquad (36)$$

$$f_{F2} = \left(1 - \exp\left(-\frac{y^+}{25}\right)\right)^4 \qquad (37)$$

The model was initially developed and calibrated using DNS data for 18% drag reduction. Subsequently it was corrected to 37% drag reduction with minor adjustments in the numerical

values of the coefficients C_{F4} and C_{ε_F}, which is a good sign regarding the robustness of the model. The model is written in expanded form in Appendix II.

3.2.6. The full NLT_{ij} model for first order turbulence closures

The model of Eq. (35) relies on the anisotropic Reynolds stress tensor, hence it can be used with second order and some first order turbulence closures. However, it has to be modified for use with isotropic first order turbulence models, such as the k–ε or the k–ω models, where the Reynolds stress is closed with the Boussinesq model of Eq. (13) implying that $\overline{u_1u_1} = \overline{u_2u_2} = \overline{u_3u_3} = 2k/3$. In this case the NLT_{ij} closure is given by Eq. (38), which has a similar form of Eq. (35) with adjustment to the numerical values of the coefficients and some of its functions. Therefore, its coefficients are now $C_{F1} = 0.32$, $C_{F2} = 5$, $C_{F3} = 0.026$, $C_{F4} = 0.81$ and $C_{\varepsilon_F} = 1.43$, the damping function f_{F2} remains the same and function f_{F1} is slightly modified to that of Eq. (39).

$$
\begin{aligned}
NLT_{ij} &\equiv \overline{c_{kj}\frac{\partial u_i}{\partial x_k}} + \overline{c_{ik}\frac{\partial u_j}{\partial x_k}} \\
&\approx C_{F1}\times\frac{C_{ij}\times f(C_{mm})}{\lambda} - \frac{C_{F2}}{We_{\tau 0}}\left[C_{kj}\frac{\partial U_i}{\partial x_k} + C_{ik}\frac{\partial U_j}{\partial x_k}\right] \\
&\quad + \frac{\lambda}{f(C_{mm})}\left[C_{F3}\times\left(\frac{\partial U_j}{\partial x_n}\frac{\partial U_m}{\partial x_k}C_{kn}\frac{\overline{u_iu_m}}{v_0\sqrt{2S_{pq}S_{pq}}}\right.\right. \\
&\quad + \frac{\partial U_i}{\partial x_n}\frac{\partial U_m}{\partial x_k}C_{kn}\frac{\overline{u_ju_m}}{v_0\sqrt{2S_{pq}S_{pq}}} \\
&\quad \left.\left. + \frac{\partial U_k}{\partial x_n}\frac{\partial U_m}{\partial x_k}\left(C_{jn}\frac{\overline{u_iu_m}}{v_0\sqrt{2S_{pq}S_{pq}}} + C_{in}\frac{\overline{u_ju_m}}{v_0\sqrt{2S_{pq}S_{pq}}}\right)\right)\right] \\
&\quad - \frac{\lambda}{f(C_{mm})}\times f_{F1}\times C_{F4}\times\left(\frac{We_{\tau 0}}{25}\right)^{0.23} \\
&\quad \times\left[C_{jn}\frac{\partial U_k}{\partial x_n}\frac{\partial U_i}{\partial x_k} + C_{in}\frac{\partial U_k}{\partial x_n}\frac{\partial U_j}{\partial x_k} + C_{kn}\frac{\partial U_j}{\partial x_n}\frac{\partial U_i}{\partial x_k} + C_{kn}\frac{\partial U_i}{\partial x_n}\frac{\partial U_j}{\partial x_k}\right] \\
&\quad + \frac{\lambda}{f(C_{mm})}\left[\frac{C_{\varepsilon_F}}{We_{\tau 0}}\frac{4}{15}\times\frac{\varepsilon^N}{v_s\times\beta}C_{mm}\times f_{F2}\times\delta_{ij}\right]
\end{aligned}
\tag{38}
$$

$$
f_{F1} = \left(1 - 0.8\exp\left(-\frac{y^+}{30}\right)\right)^2 \tag{39}
$$

A final modification to this model is necessary as discussed in the next section, but first we briefly assess the performance of the general closure for second order turbulence model (Eq. (35) and Appendix II plotted as full lines) and of the isotropic turbulence NLT_{ij} closure of Eq. (38) in dashed lines in comparison with DNS data (symbols) in Fig. 10(a)–(d). The quantities appearing in the model equations are also obtained from DNS, so only the closure for NLT_{ij} is being assessed here.

Generally, the "second order" model predicts well both LDR and IDR, but we must distinguish between the viscous sublayer region and the buffer and log-law regions. NLT_{ij} in the viscous sublayer is not so important, because other terms in the governing equations are much larger than this contribution [8] and the discrepancies in the near-wall region are essentially of no consequence. In the buffer and log-law regions the model performs well with a slight overprediction of NLT_{11} and a slight shift in the location of the peak value of NLT_{22} towards the wall. The model underpredicts NLT_{33} and for NLT_{12} the model behaves very well in the outer region but underpredicts in the inner region.

The performance of the isotropic NLT_{ij} model is equally good. NLT_{11} is not so well predicted as by the second order model especially at IDR and for NLT_{22} and NLT_{33} there are minor improvements at some locations. Regarding the shear component the isotropic model performed better than the general model in the log-law region, but is worse in the inner region. The two models are similar at LDR and show different behaviour at IDR, with the isotropic model deviating more from the DNS data and performing less well. This can be justified by the increase of anisotropic effects with drag reduction, something that is not well captured by the isotropic NLT_{ij} model.

As DR increases, both models capture well the shift away from the wall of the peaks of the various components of NLT_{ij}. In the context of a two-equation turbulence model the most important component of NLT_{ij} is NLT_{22}, which strongly affects C_{22} since the other terms in the evolution equation of C_{22} are null. Then, this affects the polymer shear stress τ^p_{12} and the momentum equation. In the governing equations of the other stresses, such as τ^p_{11} the other exact terms of τ^p_{11} far outweigh NLT_{11}, even though NLT_{11} is the largest component of NLT_{ij}. The capacity of this turbulence model to predict the negative peak of NLT_{11} in the near wall region contributes to a correct prediction of C_{kk}, and more specifically to the increase of its near wall peak with drag reduction, cf. Fig. 3.

These two NLT_{ij} models, and in particular the second order version, are good at predicting NLT_{kk}, but these comparisons are not shown since we are not using any of these model forms.

3.2.7. Summary of NLT_{ij} closure with isotropic turbulence for first order turbulence closures

The NLT_{ij} closures presented above, Eqs. (35) and (38), were developed on the basis of the DNS data, but they are to be used in the context of turbulence closures which themselves are based on simplifying assumptions. When using the NLT_{ij} closure within the scope of a k–ε model the assumption of turbulence isotropy in the latter will naturally affect the performance of the former, since the turbulence is not isotropic and the prediction of k will not necessarily match the distribution of k from DNS. For this reason minor modifications to the above NLT_{ij} closures are necessary for it to work properly when integrated in a specific turbulence closure, as the k–ε model used here. These are modifications in the numerical values of the parameters and the introduction of the polymeric viscosity in the last term of the closure, everything else remaining unchanged. Hence, the final form of the NLT_{ij} closure implemented in the present viscoelastic k–ε turbulent model is given by Eq. (40).

$$
\begin{aligned}
NLT_{ij} &\equiv \overline{c_{kj}\frac{\partial u_i}{\partial x_k}} + \overline{c_{ik}\frac{\partial u_j}{\partial x_k}} \\
&\approx C_{F1}\left(0.055\frac{We_{\tau 0}}{25} + 0.12\right)\times\frac{C_{ij}\times f(C_{mm})}{\lambda} \\
&\quad - C_{F2}We_{\tau 0}^{0.74}\left[C_{kj}\frac{\partial U_i}{\partial x_k} + C_{ik}\frac{\partial U_j}{\partial x_k}\right] \\
&\quad + \frac{\lambda}{f(C_{mm})}\left[C_{F3}\times\left(\frac{25}{We_{\tau 0}}\right)^{0.72}\times\left(\frac{\partial U_j}{\partial x_n}\frac{\partial U_m}{\partial x_k}C_{kn}\frac{\overline{u_iu_m}}{v_0\sqrt{2S_{pq}S_{pq}}}\right.\right. \\
&\quad + \frac{\partial U_i}{\partial x_n}\frac{\partial U_m}{\partial x_k}C_{kn}\frac{\overline{u_ju_m}}{v_0\sqrt{2S_{pq}S_{pq}}} \\
&\quad \left.\left. + \frac{\partial U_k}{\partial x_n}\frac{\partial U_m}{\partial x_k}\left(C_{jn}\frac{\overline{u_iu_m}}{v_0\sqrt{2S_{pq}S_{pq}}} + C_{in}\frac{\overline{u_ju_m}}{v_0\sqrt{2S_{pq}S_{pq}}}\right)\right)\right] \\
&\quad - \frac{\lambda}{f(C_{mm})}\times f_{F1}\times C_{F4}\times\left(\frac{25}{We_{\tau 0}}\right)^{0.7} \\
&\quad \times\left[C_{jn}\frac{\partial U_k}{\partial x_n}\frac{\partial U_i}{\partial x_k} + C_{in}\frac{\partial U_k}{\partial x_n}\frac{\partial U_j}{\partial x_k} + C_{kn}\frac{\partial U_j}{\partial x_n}\frac{\partial U_i}{\partial x_k} + C_{kn}\frac{\partial U_i}{\partial x_n}\frac{\partial U_j}{\partial x_k}\right] \\
&\quad + \frac{\lambda}{f(C_{mm})}\left[\frac{C_{\varepsilon_F}}{We_{\tau 0}}\frac{4}{15}\times\frac{\varepsilon^N}{(v_s + v_{\tau_p})\times\beta}C_{mm}\times f_{F2}\times\delta_{ij}\right]
\end{aligned}
\tag{40}
$$

The numerical values of the coefficients of this NLT_{ij} closure are listed in Table 1, whereas the damping functions remain unchanged.

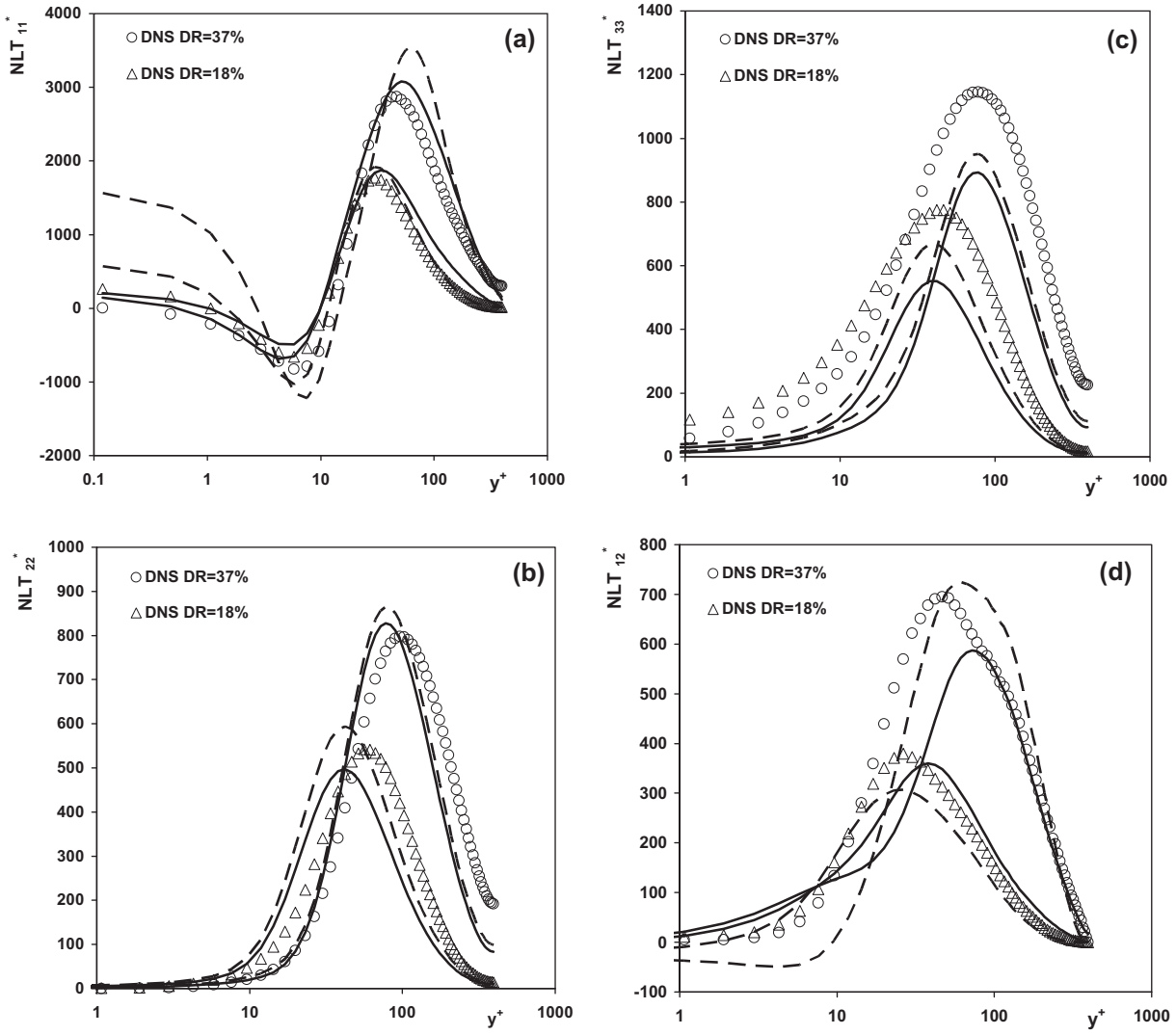

Fig. 10. Comparison between DNS data (symbols), the second-order model (—) and the isotropic model (– –) of NLT^*_{ij} and for $Re_{\tau 0} = 395$, $L^2 = 900$, $\beta = 0.9$ with $We_{\tau 0} = 25$ (DR = 18%) and $We_{\tau 0} = 100$ (DR = 37%): (a) NLT^*_{11}; (b) NLT^*_{22}; (c) NLT^*_{33}; (d) NLT^*_{12}.

4. Eddy viscosity model

Results from experiments on drag reduction [22] as well as from the DNS of Sureshkumar et al. [5] and Li et al. [8] show a reduction in the normalised Reynolds shear stress as DR is increased. This implies a reduction in the eddy viscosity. The model used by Pinho et al. [9] for the eddy viscosity is that of Jones and Launder [40], which requires an increase in ε^N to predict the correct behaviour of the Reynolds stress with drag reduction. However, this contradicts the literature regarding the behaviour of ε^N and the implication is that polymers must affect directly the distribution of the eddy viscosity, i.e., the model for v_T should directly involve quantifiers of viscoelasticity.

We propose a new closure for the eddy viscosity of the polymer solution to correct the deficiencies of the previous model of Pinho et al. [9], which was essentially identical to that for a Newtonian fluid. This new closure is Eq. (41) and contains a polymer eddy viscosity (v_T^p), which is proportional to the trace of the conformation tensor and the Weissenberg number in addition to the classical quantities (k and ε^N).

$$v_T = v_T^N - v_T^p = v_T^N\left(1 - \frac{v_T^p}{v_T^N}\right) \tag{41a}$$

$$\text{with } v_T^N = C_\mu \times f_\mu \times \frac{k^2}{\tilde{\varepsilon}} \text{ and } \frac{v_T^p}{v_T^N} = C_\mu^p \times f_\mu^p \times f_{DR} \times \frac{C_{mm}}{\sqrt{L^2 - 3}} \tag{41b}$$

The damping function f_μ^p accounts for the different damping of the wall acting on the polymer eddy viscosity and f_{DR} introduces a Weissenberg number effect, both given in Eqs. (42a) and (42b). Here, and elsewhere in the turbulence model, we adopt the model of Nagano and Hishida [41] for the terms common to the corresponding turbulence model for a Newtonian fluid, such as for the classical Van Driest damping function [42] for the eddy viscosity f_μ, given in Eq. (42c), and for the coefficient $C_\mu = 0.09$. The new coefficient $C_\mu^p = 0.0135 \times \left[\frac{25}{We_{\tau 0}}\right]^{0.12}$ and the function f_μ^p, accounting for viscoelastic effects near the wall, was calibrated using DNS data, in a way similar to that of the viscous damping function f_μ [36]. The f_{DR} function corrects the elastic contribution to the energy balance at small Weissenberg numbers.

$$f_\mu^p = \left[1 + 2.55 \times \exp\left(-\frac{y^+}{44}\right)\right] \tag{42a}$$

$$f_{DR} = \left[1 - \exp\left(-\frac{We_{\tau 0}}{6.25}\right)\right]^4 \tag{42b}$$

$$f_\mu = \left[1 - \exp\left(-\frac{y^+}{26.5}\right)\right]^2 \tag{42c}$$

The transverse variation of the DNS polymer eddy viscosity is compared with the model of Eq. (41b) in Fig. 11, whereas the total eddy viscosity data are compared in Fig. 12. In both figures the model data corresponds to the predictions by the k–ε model. The new turbulent viscosity model has a strong impact in the buffer and log layers, and it has an important role to correctly predict the shear stresses and the rate of dissipation as will be shown in Section 6. The discrepancy observed between the model predictions and the DNS data in the inertial layer is typically found also for Newtonian fluids especially at low Reynolds number turbulence, where the DNS at the edge of the outer region shows intermittency effects and a stronger reduction of k^2 than of ε, which is absent from the k–ε theory.

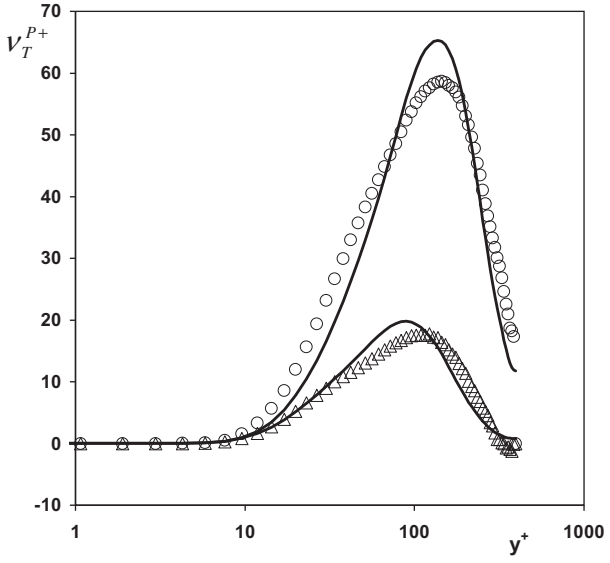

Fig. 11. Comparison between DNS data (symbols) and the model predictions (lines) of the polymeric turbulent viscosity, v_T^p, normalised by zero shear rate kinematic viscosity, v_0, defined by Eq. (41b) for turbulent channel flow with $Re_{\tau 0} = 395$, $L^2 = 900$ and $\beta = 0.9$: △, 18% DR and ○, 37% DR.

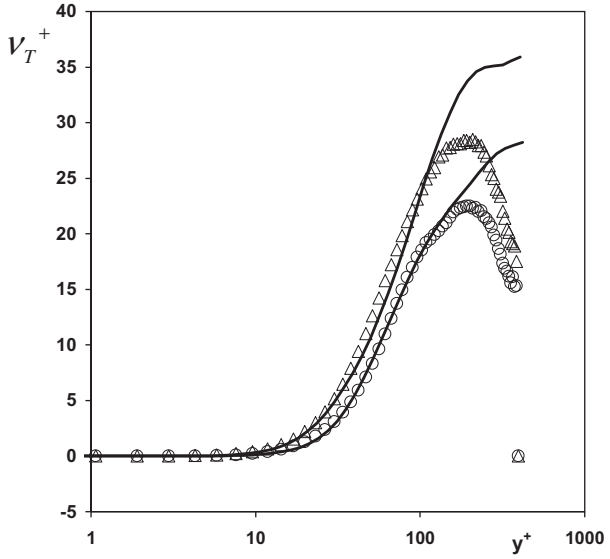

Fig. 12. Comparison between DNS data (symbols) and the turbulence model predictions (lines) of the turbulent viscosity v_T normalised by zero shear rate kinematic viscosity, v_0, for DR = 18% (△) and 37% (○) in a turbulent channel flow with $Re_{\tau 0} = 395$, $L^2 = 900$ and $\beta = 0.9$.

5. Closures in the transport equations of k and ε^N

The turbulent kinetic energy is given by its transport equation and contains terms that need to be modelled in addition to existing terms modelled in the context of Newtonian fluid mechanics that may need to be modified. One of its terms is the rate of dissipation of turbulent kinetic energy by the Newtonian solvent ($\widetilde{\varepsilon}^N$), which is also given by a transport equation, the exact form of which is Eq. (16) derived by Pinho et al. [9] for a polymer solution. In this work we adopt classical Newtonian closures as much as possible and describe the closures of terms containing viscoelastic contributions, or classical terms that are modified by the presence of the polymer additives. As a consequence the transport equations for k and $\widetilde{\varepsilon}^N$ that we actually solve are Eqs. (43) and (44), respectively.

$$\frac{\partial \rho k}{\partial t} + \frac{\partial \rho U_i k}{\partial x_i} = \frac{\partial}{\partial x_i}\left[\left(\eta_s + \frac{\rho f_t v_T}{\sigma_k}\right)\frac{\partial k}{\partial x_i}\right] - \rho\overline{u_i u_k}\frac{\partial U_i}{\partial x_k} - \rho\left(\widetilde{\varepsilon}^N + D\right) + Q^V - \rho\varepsilon^V \tag{43}$$

$$\frac{\partial \rho \widetilde{\varepsilon}^N}{\partial t} + \frac{\partial \rho U_i \widetilde{\varepsilon}^N}{\partial x_i} = \frac{\partial}{\partial x_i}\left[\left(\eta_s + \frac{\rho f_t v_T}{\sigma_\varepsilon}\right)\frac{\partial \widetilde{\varepsilon}^N}{\partial x_i}\right] + f_1 C_{\varepsilon_1}\frac{\widetilde{\varepsilon}^N}{k}P_k - f_2 C_{\varepsilon_2}\rho\frac{\widetilde{\varepsilon}^{N^2}}{k} + \eta_s v_T(1 - f_\mu)\left(\frac{\partial^2 U_i}{\partial y \partial y}\right)^2 + E_{\tau_p} \tag{44}$$

$$D = 2\left(v_s + v_{\tau p}\right)\left(\frac{d\sqrt{k}}{dy}\right)^2 \tag{45}$$

The l.h.s. of Eqs. (43) and (44) concern the advection of the transported quantities. The first term on the r.h.s. of both equations account for turbulent diffusion of the transported quantities, here modelled as for Newtonian fluids following Nagano and Hishida [41], but modified by a variable turbulent Prandtl number via function f_t to correct turbulent diffusion near the wall as suggested by Nagano and Shimada [43] and Park and Sung [44] ($f_t = 1 + 3.5\exp\left[-(R_T/150)^2\right]$ with $R_T = k^2/(v_s\widetilde{\varepsilon}^N)$). We also follow the standard approach of working with a modified Newtonian rate of dissipation of k ($\widetilde{\varepsilon}^N$), related to the true dissipation (ε^N) by $\varepsilon^N = \widetilde{\varepsilon}^N + D$, where D is given in Eq. (45). Regarding D, it was necessary to account for the shear-thinning of the FENE-P model by using the solution viscosity, which is the sum of the solvent kinematic viscosity (v_s) with the local polymer kinematic viscosity given by $v_{\tau_p} = \overline{\tau}_{xy}^p/(\rho\dot{\gamma})$, where $\dot{\gamma}$ is the local shear rate.

The final terms on the r.h.s. of Eqs. (43) and (44) introduce the polymer effect; the two last terms in Eq. (43) are the viscoelastic turbulent transport (Q^V) and the viscoelastic stress work (ε^V), whereas the last term in Eq. (44) (E_{τ_p}) is the viscoelastic contribution to the equation of $\widetilde{\varepsilon}_N$, which we call the viscoelastic destruction of dissipation. The remaining terms are those of the base Newtonian turbulence model, as mentioned above, and the corresponding damping functions taking account of the low Reynolds number behaviour are $f_\mu = [1 - \exp(-y^+/26.5)]^2$, with $y^+ = u_\tau y/v_{wall}$ based on the wall kinematic viscosity of the solution, $f_1 = 1.0$ and $f_2 = 1 - 0.3\exp\left(-R_T^2\right)$. The numerical values of the remaining coefficients are: $\sigma_k = 1.1$, $\sigma_\varepsilon = 1.3$, $C_{\varepsilon_1} = 1.45$ and $C_{\varepsilon_2} = 1.90$.

To finalise the turbulence model we present below the closures developed for ε^V, Q^V and E_{τ_p}.

5.1. Viscoelastic stress work model

The viscoelastic stress work is defined as

$$\varepsilon^V = -\frac{\eta_p}{\rho\lambda}\left[C_{ik}\overline{f(C_{mm}+c_{mm})\frac{\partial u_i}{\partial x_k}} + \overline{c_{ik}f(C_{mm}+c_{mm})\frac{\partial u_i}{\partial x_k}}\right] \tag{46}$$

and needs to be modelled.

For DR = 18% Pinho et al. [9] have shown that the double correlation is negligible by comparison with the triple correlation, $C_{ik}\overline{f(\widehat{c}_{mm})\frac{\partial u_i}{\partial x_k}} \ll \overline{c_{ik}f(\widehat{c}_{mm})\frac{\partial u_i}{\partial x_k}}$ and the same applies at IDR, even though by a slight lesser amount as can be seen in Fig. 13. As the Weissenberg number increases the magnitude of the double correlation term increases in absolute and relative terms, but far from the wall the underlying approximation essentially remains valid.

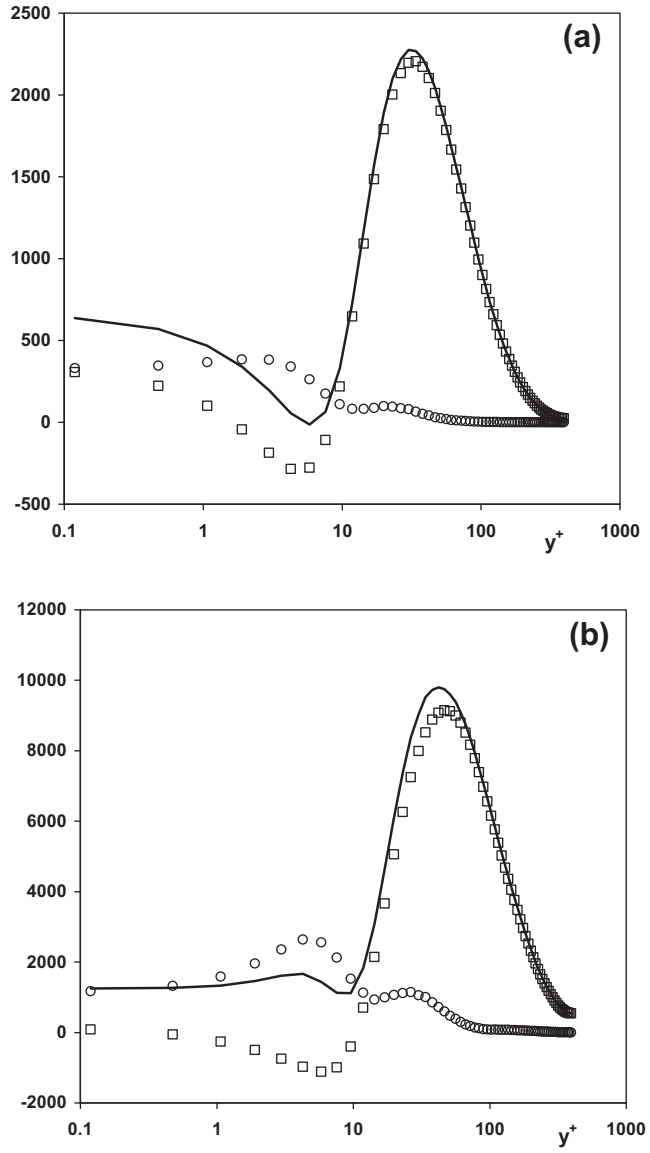

Fig. 13. Transverse profiles of the different contributions to $\varepsilon^{V^+}Re_{\tau 0}^2$ (Eq. (46)), (○) $C_{ik}\overline{f(C_{mm}+c_{mm})\frac{\partial u_i}{\partial x_k}}$, (□) $\overline{c_{ik}f(C_{mm}+c_{mm})\frac{\partial u_i}{\partial x_k}}$ and the sum (—) for the channel flow of a FENE-P with Re_τ = 395, L^2 = 900, β = 0.9: (a) $We_{\tau 0}$ = 25, DR = 18% and (b) $We_{\tau 0}$ = 100, DR = 37%.

Close to the wall the double correlation is as important as the triple correlation, but ε^V is negligible in comparison to three other relevant terms of the transport equation of k, namely the rate of dissipation by the Newtonian solvent, the production of turbulence and the molecular diffusion of k, cf. Pinho et al. [9]. Therefore the same simplification, embodied in Eq. (47), can be used at IDR with no negative effects upon the balance equation of k.

$$\varepsilon^V \approx \frac{\eta_p}{\rho\lambda}\left[\overline{c_{ik}f(C_{mm}+c_{mm})\frac{\partial u_i}{\partial x_k}}\right] \tag{47}$$

Following the methodology of Pinho et al. [9], the triple correlation is decoupled into a product of function $f(C_{kk})$ by the remaining double correlation which is none other than NLT_{kk}, and corrected by a multiplicative parameter. To account for a small Weissenberg number dependence a corrective function is also introduced leading to the final form of the model for the viscoelastic stress work given by Eq. (48), where $C_{\varepsilon^V} = 1.27$ and $n = 1.15$.

$$\begin{aligned}\varepsilon^V &\simeq \frac{\eta_p}{\rho\lambda}\left[\overline{c_{ik}f(C_{mm}+c_{mm})\frac{\partial u_i}{\partial x_k}}\right] \approx \frac{\eta_p}{\rho\lambda}\left[f(C_{mm})\overline{c_{ik}\frac{\partial u_i}{\partial x_k}}\right] \\ &= C_{\varepsilon^V}\left(\frac{We_{\tau 0}}{25}\right)^{n-1}\frac{\eta_p}{\rho\lambda}\left[f(C_{mm})\frac{NLT_{mm}}{2}\right]\end{aligned} \tag{48}$$

Therefore, NLT_{ij} plays a second role, this time modelling the viscoelastic stress work appearing in the transport equation of turbulence kinetic energy via its trace. Hence, it is important for the closure developed for NLT_{ij} to be able to predict accurately its trace, NLT_{kk}.

In Fig. 14 four sets of data are plotted: the DNS data for ε^V, the predictions by the model of Eq. (48) using directly the DNS data for NLT_{kk} and the predictions of Eq. (48) using the NLT_{kk} as given by the two closures developed in Sections 3.2.5 and 3.2.6. The model of Eq. (48) is good where it should be, i.e., in the buffer and log law layers and that the correct prediction of the viscoelastic stress work in these regions requires a good prediction of NLT_{kk}. The use of the "isotropic" NLT_{kk} model does not lead to such a good prediction as the general NLT_{ij} closure, but it is still satisfactory. The discrepancy between ε^V and any of the models in the viscous sublayer is of no consequence, given the negligible impact of ε^V in the balance of k in this region.

However, the final form of the model for the viscoelastic stress work, to be used with the NLT_{ij} model of Section 3.2.7 ((40)), is the following modification of the LDR model of Pinho et al. [9], here extended to IDR

$$\varepsilon^V \equiv \frac{1}{\rho}\overline{\tau_{ik}'^p\frac{\partial u_i}{\partial x_k}} \approx 1.37 \times \left[\frac{We_{\tau 0}}{25}\right]^{0.1} \times f_{DR}\frac{\eta_p}{\rho\lambda}f(C_{mm})\frac{NLT_{mm}}{2} \tag{49}$$

The modification of ε^V is embodied by function f_{DR}, Eq. (42b), which corrects the coefficient 1.37 to take into account its nonlinear dependence on the Weissenberg number.

5.2. Viscoelastic turbulent transport model

The viscoelastic turbulent transport, Q^V, is exactly given by

$$\begin{aligned}Q^V &= \frac{\eta_p}{\lambda}\frac{\partial}{\partial x_k}\left[(CU)_{iik} + C_{ik}(FU)_i\right] \\ &= \frac{\eta_p}{\lambda}\frac{\partial}{\partial x_k}(CU)_{iik} + \frac{\eta_p}{\lambda}\frac{\partial}{\partial x_k}\left[C_{ik}(FU)_i\right]\end{aligned} \tag{50}$$

where $(CU)_{iik} = \overline{c_{ik}f(\widehat{c}_{mm})u_i}$ and $(FU)_i = \overline{f(\widehat{c}_{mm})u_i}$. Although it is not very important at LDR, Pinho et al. [9] developed a closure for Q^V neglecting the effect of the double correlation and modelling only the triple correlation. However, the double correlation becomes important as DR increases, as is shown in Fig. 15, where $\overline{c_{ik}f(\widehat{c}_{mm})u_i} + C_{ik}\overline{f(\widehat{c}_{mm})u_i}$ and $\overline{c_{ik}f(\widehat{c}_{mm})u_i}$ are plotted. The difference

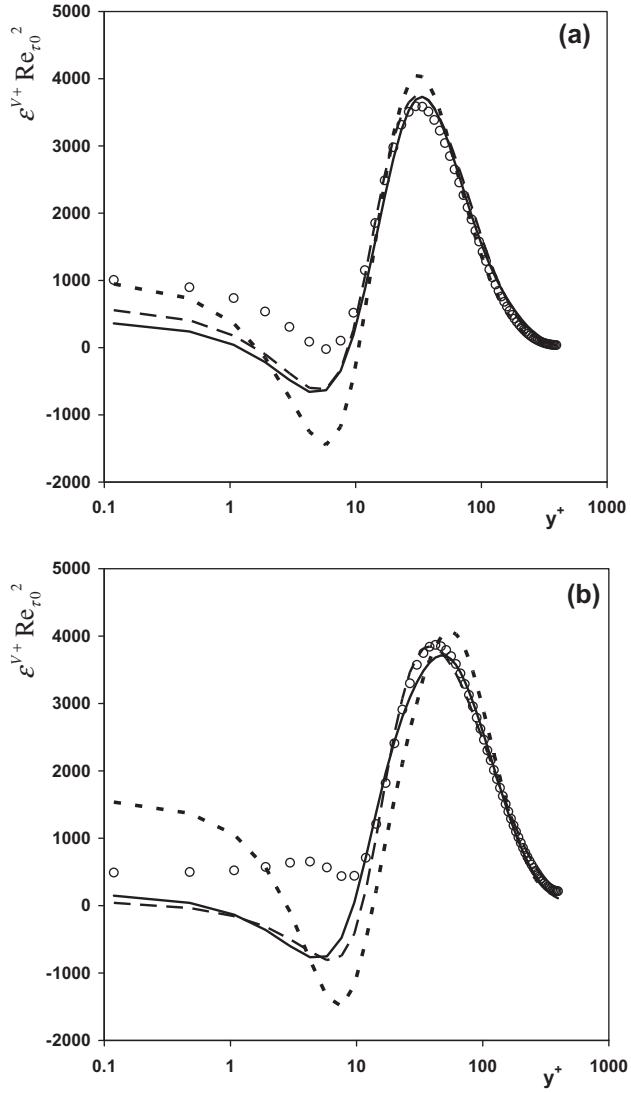

Fig. 14. Comparison between DNS data of $\varepsilon^{V^+} Re_{\tau 0}^2$ (○) and the models of Eq. (48) using NLT_{kk}^* DNS data (– – –), NLT_{kk}^* from the second-order NLT_{ij}^* model (—) and from the "isotropic" NLT_{ij}^* model (■ ■ ■) for $Re_{\tau 0} = 395$, $L^2 = 900$ and $\beta = 0.9$ as a function of drag reduction: (a) $We_{\tau 0} = 25$ (18% DR) and (b) $We_{\tau 0} = 100$ (37% DR).

between the two quantities corresponds to $C_{ik}\overline{f(\hat{c}_{mm})u_i}$, which increases significantly when DR rises from 18% to 37%. In this work we provide a new closure for Q^V incorporating a modification to the model of $(CU)_{iik}$ developed by Pinho et al. [9] to account for Weissenberg number effects, and the new model for $(FU)_i$, which is developed below.

A fluctuating strain rate is usually related to turbulent velocity and length scales, but for the purpose of modelling the viscoelastic turbulent transport we consider instead a viscoelastic turbulent length scale ($L_\lambda \sim u\lambda$), defined as the length travelled by a fluid particle due exclusively to the fluctuating turbulent flow for a period of the order of the relaxation time of the polymer.

$$\frac{\partial u}{\partial x} \sim \frac{u}{L_\lambda} \rightarrow u \sim L_\lambda \frac{\partial u}{\partial x} \rightarrow u \sim \lambda u \frac{\partial u}{\partial x} \tag{51}$$

Estimating

$$\overline{f(\hat{c}_{mm})u} \sim \lambda \times \overline{f(\hat{c}_{mm})u \frac{\partial u}{\partial x}} \tag{52}$$

since by definition

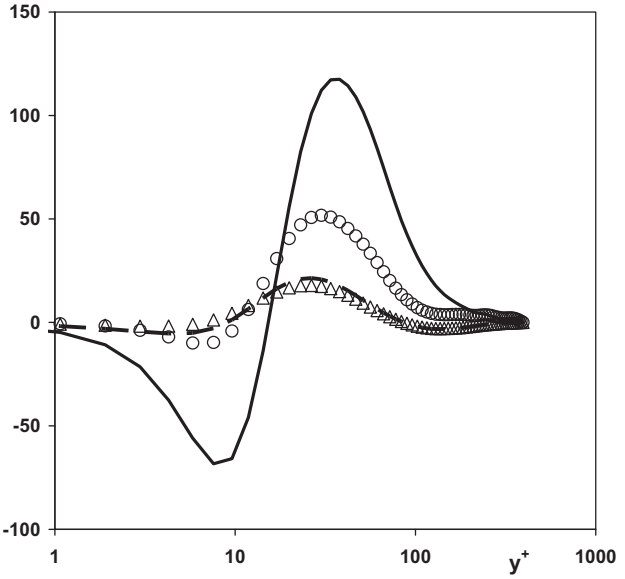

Fig. 15. Comparison between DNS data of $\overline{c_{ik}f(C_{mm}+c_{mm})u_i^+}$ (symbols) and $\overline{c_{ik}f(C_{mm}+c_{mm})u_i^+} + C_{ik}\overline{f(C_{mm}+c_{mm})u_i^+}$ (lines) for channel flow of a FENE-P at $Re_\tau = 395$, $L^2 = 900$ and $\beta = 0.9$: (– –) and (△) for $We_\tau = 25$, DR = 18%; (—) and (○) for $We_\tau = 100$, DR = 37%.

$$2\overline{u_i \frac{\partial u_i}{\partial x_j}} = \frac{\partial \overline{u_i u_i}}{\partial x_j} \tag{53}$$

and considering that $\sqrt{\overline{c_{kk}^2}} \ll C_{kk}$ and the arguments in Section 3.1 on the behaviour of function $f(\hat{c}_{mm})$, our proposal for the model of $(FU)_i$ is Eq. (54). We arrived at this model using Eq. (52), then decoupling to bring $f(\hat{c}_{mm})$ out of the cross-correlation and applying Eq. (53).

$$(FU)_i = \overline{f(\hat{c}_{mm})u_i} \approx \frac{C_{FU}}{2} \times \lambda \times f(C_{mm}) \times \frac{\partial \overline{u_n u_n}}{\partial x_i} \tag{54}$$

Calibration against the DNS data provides the numerical value of $C_{FU} = 1$ and introduces a Weissenberg number correction that makes this double correlation larger as the Weissenberg number increases (cf. Fig. 15) so that the final form of the model for the second term inside the derivative on the r.h.s. of Eq. (50) is Eq. (55) with $C_{FU} = 0.5$.

$$C_{ik}(FU)_i = \frac{C_{FU}}{2}\sqrt{\frac{We_{\tau 0}}{25}} \times C_{ik} \times \lambda \times f(C_{mm}) \times \frac{\partial \overline{u_n u_n}}{\partial x_i} \tag{55}$$

The model of Pinho et al. [9] for $(CU)_{iik}$ is a contraction of their more general model for $(CU)_{ijk}$. It was extended to IDR by incorporating a Weissenberg number dependence and is given by

$$(CU)_{ijk} = -C_{\beta 1}\sqrt{\frac{25}{We_{\tau 0}}}\frac{\lambda}{f(C_{mm})}\left(\overline{u_i u_m}\frac{\partial C_{kj}}{\partial x_m} + \overline{u_j u_m}\frac{\partial C_{ik}}{\partial x_m}\right) - C_{\beta 2}\left(\frac{We_{\tau 0}}{25}\right)^{1.66}\left[\pm\sqrt{\overline{u_j^2}}C_{ik} \pm \sqrt{\overline{u_i^2}}C_{jk}\right] \tag{56}$$

with parameters $C_{\beta 1} = 0.6$ and $C_{\beta 2} = 0.05$.

The performance of the full closure for $(CU)_{iik} + C_{ik}(FU)_i$ against DNS data is shown in Fig. 16 for 18% and 37% of drag reduction. The model compares well with the DNS data and captures its main features. A small shift is observed in the sloping increase in the buffer layer at DR = 37%, but the impact of this is negligible since Q^V is not a major term in the balance of turbulent kinetic energy.

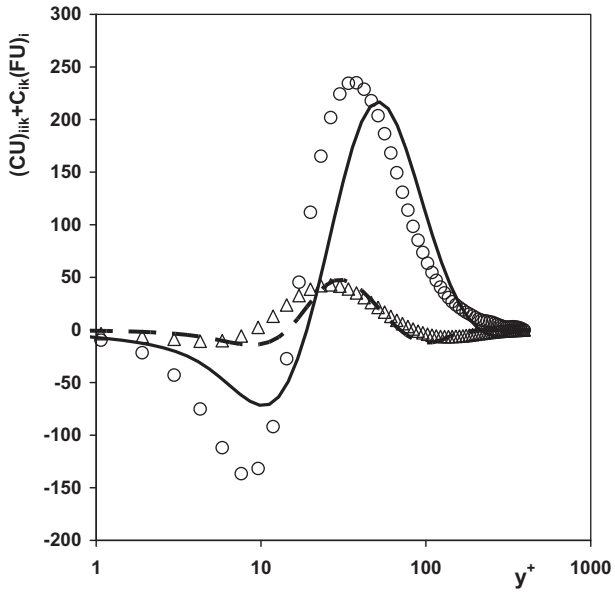

Fig. 16. Comparison between model predictions of $(CU)_{iik} + C_{ik}(FU)_i$ (lines) and DNS data (symbols) for channel flow of FENE-P fluids at $Re_\tau = 395$, $L^2 = 900$ and $\beta = 0.9$: (– –) and (△) for $We_\tau = 25$, DR = 18%; (—) and (○) for $We_\tau = 100$, DR = 37%.

5.3. Model for the viscoelastic destruction of the Newtonian rate of dissipation

Previous models for viscoelastic fluids [7–9] neglected the extra term E_{τ_p} appearing in the transport equation of $\widetilde{\varepsilon}^N$ for viscoelastic fluids. One of the consequences for the model of Pinho et al. [9] was an overprediction of $\widetilde{\varepsilon}^N$, a partial contribution to an underprediction of k and some deficiencies in the prediction of $-\overline{uv}$. The reduction of $\widetilde{\varepsilon}^N$ with DR reported in the literature requires a direct influence of the polymer in reducing $\widetilde{\varepsilon}^N$, which formally exists as term E_{τ_p}. Therefore we assume that E_{τ_p} is a destruction type term in order to allow the model to reduce $\widetilde{\varepsilon}^N$. A major contribution of this work is exactly in providing, for the first time, a model for this new term.

In developing a model for E_{τ_p}, and assuming that it plays the role of a destruction term it was also assumed that it should depend on the same quantities as the classical Newtonian destruction term, i.e., it should be proportional to ε^2/k, with ε here representing any of the stress work terms ($\widetilde{\varepsilon}^N$ or ε^V). The viscoelastic destruction term is modelled as in Eq. (57) and has two contributions, both of which are proportional to viscoelastic quantities.

$$E_{\tau_p} = -f_5 \times f_{DR} \times \frac{(1-\beta)}{We_{\tau 0}} \times \frac{\widetilde{\varepsilon}^{N^2}}{k}\left[C_{\varepsilon F1} \times \frac{\varepsilon^V}{\widetilde{\varepsilon}^N} + C_{\varepsilon F2} \times \left(\frac{C_{mm} \times f(C_{mm})}{\left(L^2-3\right)}\right)^2\right] \tag{57}$$

This closure includes a wall damping function $f_5 = [1 - \exp(-y^+/50)]$, a Weissenberg number corrector function f_{DR}, defined before, and the numerical coefficients $C_{\varepsilon F1} = 476 \times (We_{\tau 0}/25)^{0.56}$ and $C_{\varepsilon F2} = 428 \times (25/We_{\tau 0})^{1.37}$.

5.4. Summary of the present model

It is helpful at this stage to summarise and present the complete set of equations that need to be solved to arrive at a solution for turbulent flow of a FENE-P fluid in the context of RANS/RACE model developed here. They are the equations of continuity

$$\frac{\partial U_i}{\partial x_i} = 0 \tag{58}$$

and momentum

$$\rho\frac{DU_i}{Dt} = -\frac{\partial \bar{p}}{\partial x_i} + \frac{\partial}{\partial x_k}\left[\rho(\nu_s + \nu_T)\frac{\partial U_i}{\partial x_k}\right] + \frac{\partial \overline{\tau}^p_{ki}}{\partial x_k} \tag{59}$$

where the polymer stress tensor is calculated by

$$\overline{\tau}^p_{ij} = \frac{\eta_p}{\lambda}\left[\frac{L^2-3}{L^2-C_{kk}}C_{ij} - \delta_{ij}\right] \tag{60}$$

The eddy viscosity is calculated based on the modified k–ε^N equations, where

$$\nu_T = \nu_T^N\left(1 - \frac{\nu_T^p}{\nu_T^N}\right) = C_\mu f_\mu \frac{k^2}{\widetilde{\varepsilon}^N}\left(1 - C_\mu^p f_\mu^p f_{DR}\frac{C_{ii}}{\sqrt{L^2-3}}\right) \tag{61}$$

with coefficients $C_\mu = 0.09$, $C_\mu^p = 0.0135 \times \left[\frac{25}{We_{\tau 0}}\right]^{0.12}$, and the damping functions given in Eq. (42). The turbulent kinetic energy and $\widetilde{\varepsilon}^N$ are determined by Eqs. (62) and (63), respectively

$$\rho\frac{Dk}{Dt} = \frac{\partial}{\partial x_j}\left[\left(\eta_s + \frac{\rho f_1 \nu_T}{\sigma_k}\right)\frac{\partial k}{\partial x_j}\right] + P_k - \rho\left(\widetilde{\varepsilon}^N + D + \varepsilon^V\right) + Q^V \tag{62}$$

$$\rho\frac{D\widetilde{\varepsilon}^N}{Dt} = \frac{\partial}{\partial x_j}\left[\left(\eta_s + \frac{\rho f_1 \nu_T}{\sigma_\varepsilon}\right)\frac{\partial \widetilde{\varepsilon}^N}{\partial x_j}\right] + f_1 C_{\varepsilon_1}\frac{\widetilde{\varepsilon}^N}{k}P_k - \rho f_2 C_{\varepsilon_2}\frac{\widetilde{\varepsilon}^{N^2}}{k} + E + E_{\tau_p} \tag{63}$$

with $P_k = -\rho\overline{u_i u_k}\partial U_i/\partial x_k$, $D = 2(\nu_s + \nu_{\tau p})\left(d\sqrt{k}/dy\right)^2$, $\nu_{\tau_p} = \overline{\tau}^p_{12}/dU/dy$ and $E = \eta_s \nu_T (1-f_\mu)\left(\partial^2 U/\partial y \partial y\right)^2$. The closure for ε^V is Eq. (49) and the function given below it and the closure for Q^V is Eq. (50) with the models for $C_{ik}(FU)_i$ and $(CU)_{iik}$ given by Eqs. (55) and (56), respectively. The model for the viscoelastic destruction (E_{τ_p}) is given in Eq. (57) with the corresponding coefficients and functions.

The time-average conformation tensor is determined by Eq. (64)

$$\frac{DC_{ij}}{Dt} = C_{jk}\frac{\partial U_i}{\partial x_k} + C_{ik}\frac{\partial U_j}{\partial x_k} + NLT_{ij} - \frac{\overline{\tau}^p_{ij}}{\eta_p} \tag{64}$$

and the required explicit NLT_{ij} model is given by Eq. (40), with the coefficients of Table 1, and the functions of Eq. (65).

$$f_{F1} = \left(1 - 0.8\exp\left(-\frac{y^+}{30}\right)\right)^2; \quad f_{F2} = \left(1 - \exp\left(-\frac{y^+}{25}\right)\right)^4 \tag{65}$$

The remaining coefficients and functions of the k and $\widetilde{\varepsilon}^N$ equations are described below Eq. (45).

6. Results and discussion

We evaluate the performance of the turbulence model against the two DNS data sets and also provide results of parametric studies. The numerical calculations were carried out using a finite-volume code [9] modified for the FENE-P fluid. Non-uniform meshes were used with 99 cells covering the channel width. About 8 cells were located inside each of the viscous sublayers in order to provide mesh independent results to within 0.5% for the mean velocity and the friction factor.

Fig. 17 compares the predicted velocity profiles with DNS data and includes predictions at Weissenberg numbers other than those used for calibration. The agreement with DNS data is good with improvements in the buffer layer relative to the previous model of Pinho et al. [9]. This improvement is associated with the inclusion of a polymeric contribution in the eddy viscosity model. The earlier model [9] also predicted a drag increase at low values of the Weissenberg number ($We_{\tau 0} < 20$), i.e., a profile below the log-law, and this deficiency has now been corrected as shown. Some

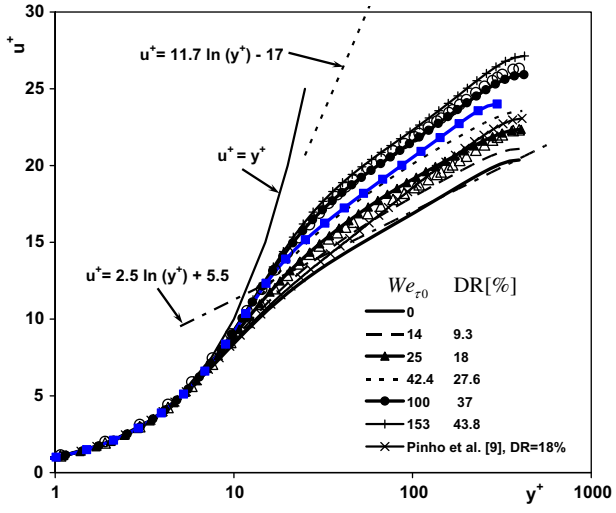

Fig. 17. Normalised velocity profile in wall coordinates for Newtonian and FENE-P flows, at $Re_{\tau 0} = 395$, $L^2 = 900$ and $\beta = 0.9$. Comparison between DNS data sets for △ 18% DR data and ○ 37% DNS data, and predictions (lines) for different Weissenberg numbers. Prediction of Iaccarino et al.'s [45] profile for $We_{\tau_0} = 36$ (DR = 31%) at $Re_{\tau 0} = 300$, $L^2 = 3600$ and $\beta = 0.9$ (blue line and ■). (For interpretation of the references to colour in this figure legend, the reader is referred to the web version of this article.)

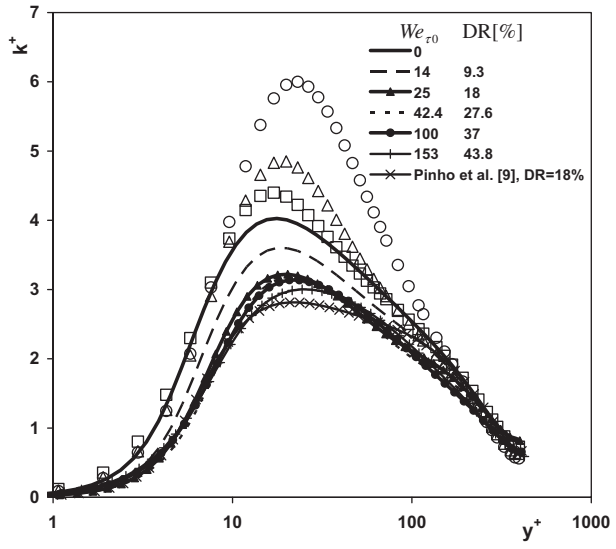

Fig. 18. Comparison between predictions (lines) and DNS (open symbols) data of the turbulent kinetic energy for turbulent channel flow with $Re_{\tau 0} = 395$, $L^2 = 900$ and $\beta = 0.9$: (□) Newtonian, (△) DR = 18% and (○) DR = 37%.

of the corresponding k^+ profiles are plotted in Fig. 18. Even though there were improvements in the prediction of the turbulent kinetic energy, this quantity is still underpredicted especially for viscoelastic fluids. The improvement is a consequence of the capacity of the new model to capture the negative part of the NLT_{11} component, which did not exist in the previous model [9], however this is not enough to reach the maximum values as in the DNS data. The underprediction problem is associated with the base turbulence model, which also underpredicts the Newtonian profile of k. We believe this deficiency is associated with the isotropic nature of this model and that the correct prediction of k needs a second order Reynolds stress model in order to capture the enhanced Reynolds stress anisotropy typical of drag reduction. Predictions at values of Weissenberg number other that those for which DNS data were collected have also been included to assess the parametric trends. For values of DR higher than 50% the model becomes numerically unstable. Further, the closures developed need to be tested against DNS data for a broader range in the parameter space of We, L^2 and β. We have carried out some preliminary investigations onto the effects of L^2 and β, and seen that enhancing the

Table 2
Comparison between prediction of drag reduction for $Re_{\tau_0} = 300, \beta = 0.9, L^2 = 3600$ and $We_{\tau_0} = 36$.

Description	Present model	Iaccarino et al. model	DNS data (Iaccarino et al. [45])
Drag reduction (%)	29	31	33

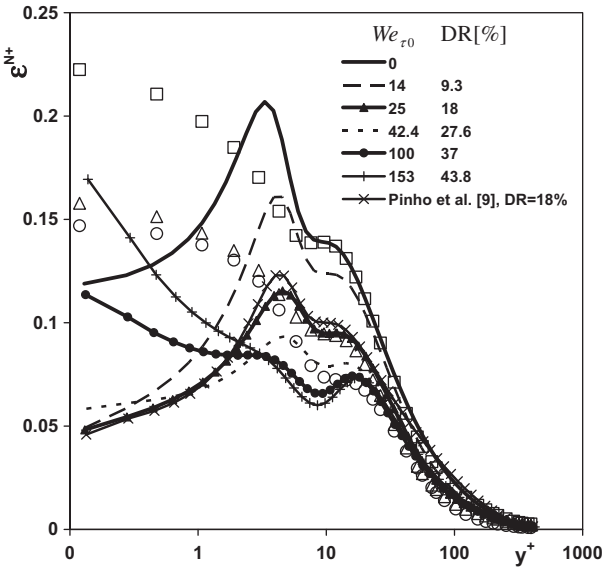

Fig. 19. Comparison between predictions (lines) and DNS (open symbols) data of ε^{N^+} for turbulent channel flow with $Re_{\tau 0} = 395$, $L^2 = 900$ and $\beta = 0.9$: (□) Newtonian, (△) DR = 18% and (○) DR = 37%.

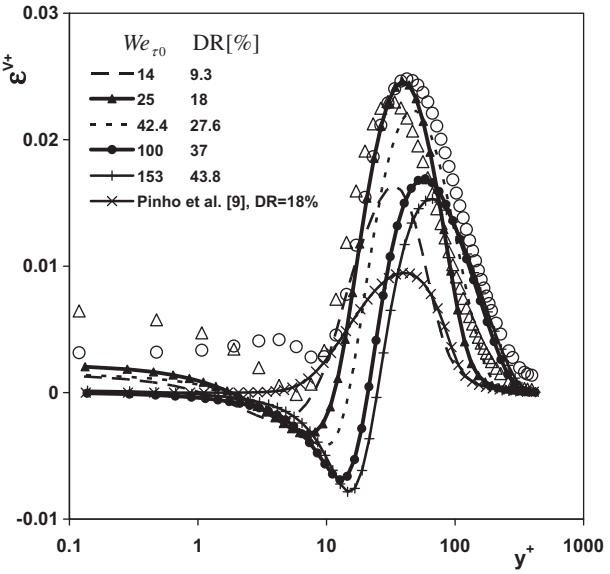

Fig. 20. Comparison between predictions (lines) and DNS (open symbols) data of ε^{V^+} for turbulent channel flow with $Re_{\tau 0} = 395$, $L^2 = 900$ and $\beta = 0.9$: (△) DR = 18% and (○) DR = 37%.

polymeric contribution by increasing L^2 by a significant amount or decreasing β results in lower predicted values of the turbulent kinetic energy. As such, the present k–ε model can be used for different values of We, L^2 and β and closely follows DNS data for

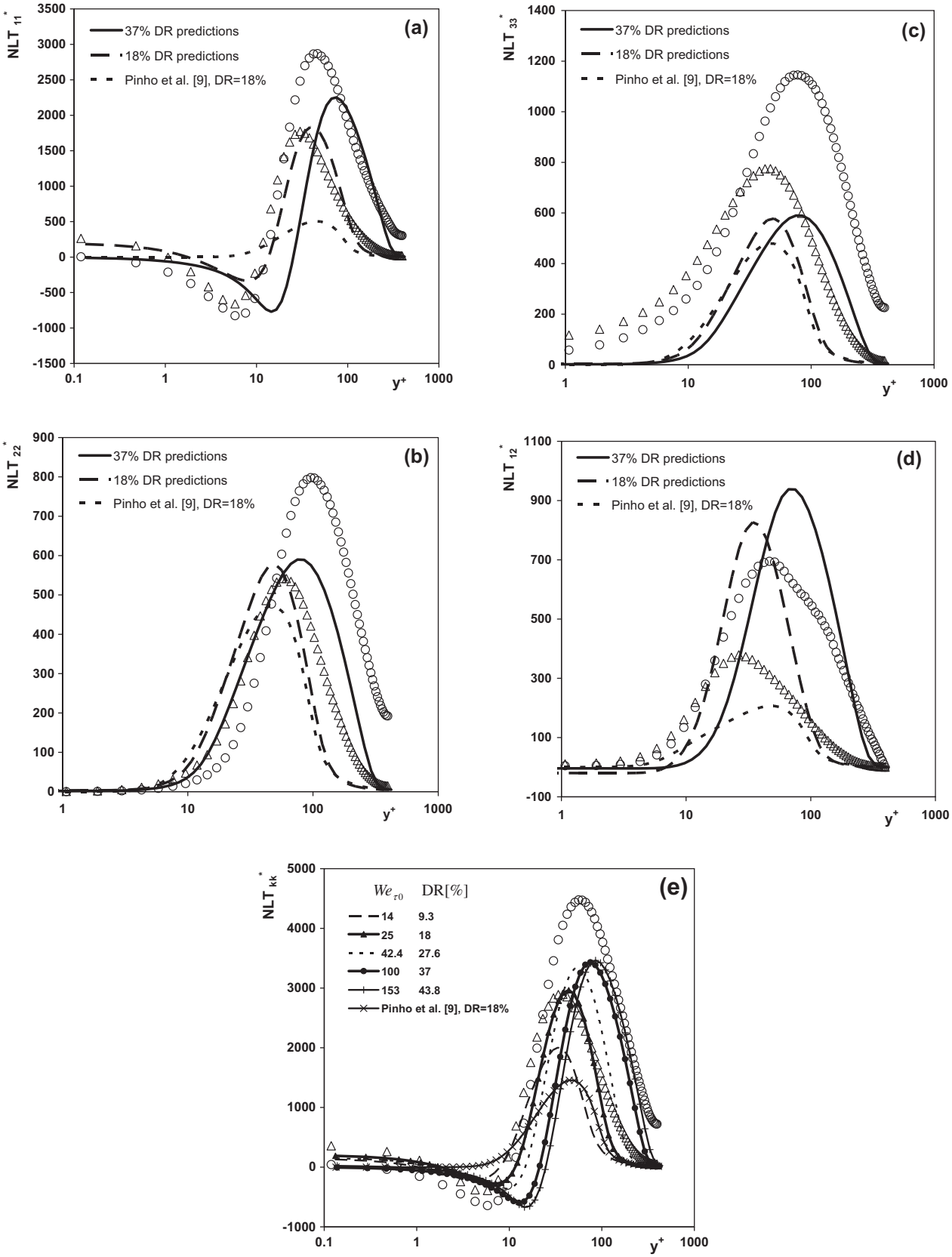

Fig. 21. Comparison between predictions (lines) and DNS (open symbols) data of NLT_{ij} for turbulent channel flow with $Re_{\tau 0} = 395$, $L^2 = 900$ and $\beta = 0.9$: (△) DR = 18% and (○) DR = 37%: (a) NLT^*_{11}; (b) NLT^*_{22}; (c) NLT^*_{33}; (d) NLT^*_{12}; (e) NLT^*_{kk}.

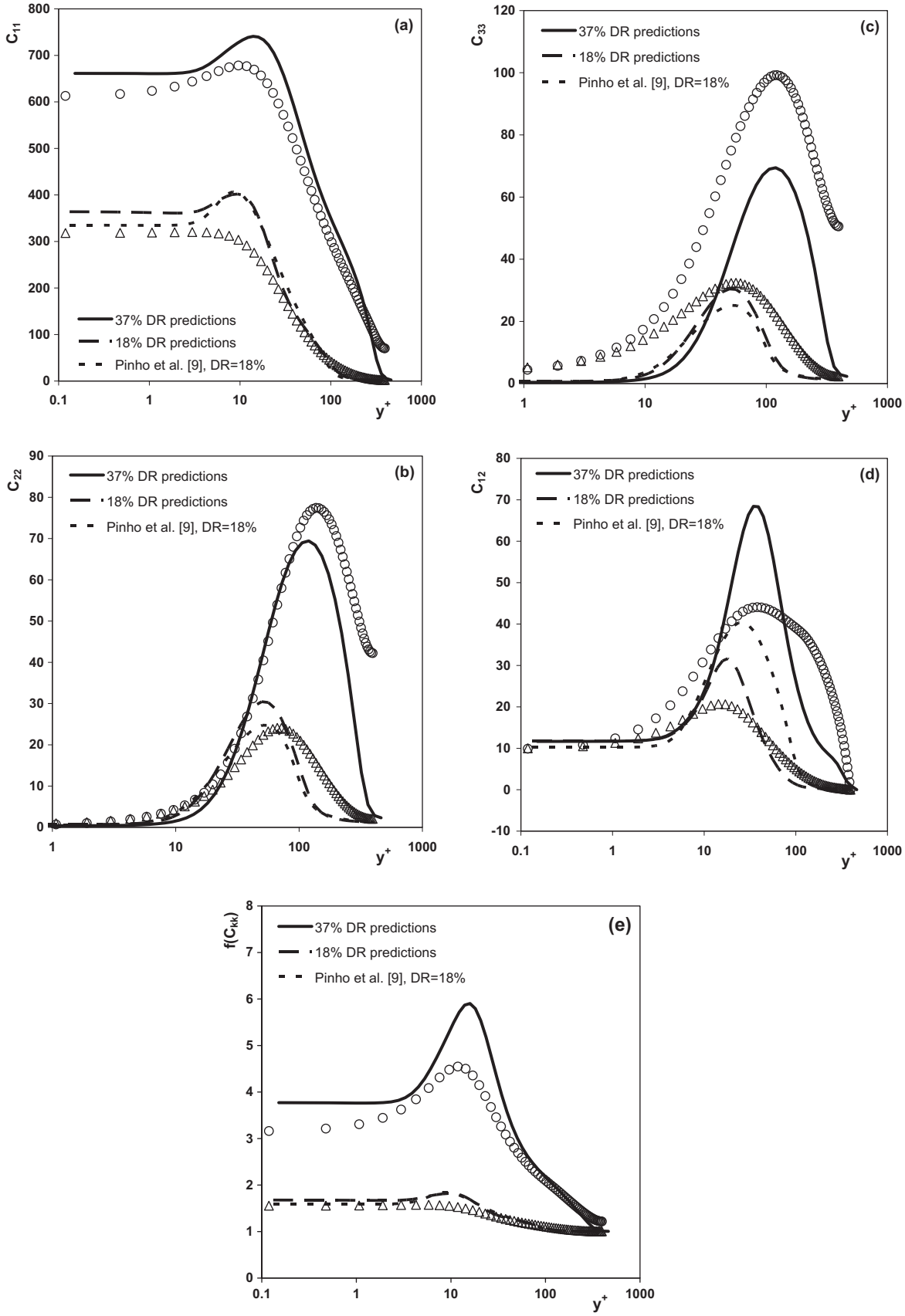

Fig. 22. Comparison between predictions and DNS data of the conformation tensor for turbulent channel flow with $Re_{\tau 0} = 395$, $L^2 = 900$ and $\beta = 0.9$: (△) DR = 18% and (○) DR = 37%.

$Re_{\tau_0} = 395$, $L^2 = 900$, $\beta = 0.9$ and $We_{\tau_0} \leqslant 153$. Based on the good behaviour of the individual viscoelastic closures developed in this work, we believe that correcting the excessive underprediction of k will enable the model to achieve higher values of drag reduction and behave properly as a function of We, L^2 and β.

For DR < 50% the tests demonstrated a good behaviour of the model and one comparison was against one flow case of Iaccarino et al. [45], which implied the use of a higher value of L^2. This set is characterised by $Re_{\tau_0} = 300$, $\beta = 0.9$, $L^2 = 3600$ and $We_{\tau_0} = 36$, Table 2 compares the corresponding prediction of drag reduction with that of Iaccarino et al. and the DNS data and the corresponding velocity profile is plotted in Fig. 17.

One of the objectives in our development of RANS models is to derive closures which are as general as possible, so that they can be used in as many RANS models as possible: as an example, the closures for NLT_{ij}, ε^V and Q^V (or ε^V_{ij} and Q^V_{ij} developed in Pinho et al. [9]) analysed below can in principle be used within the scope of k–ε, k–ω or a 2nd Reynolds stress model as is or with minimum changes, such as a simple recalibration of some parameter values (we did it for a k–ω model just by changing slightly the numerical values of two parameters). The current contribution, which involves various new closures, is therefore a significant improvement on Pinho et al. [9], but we were not able to correct completely the faulty prediction of turbulent kinetic energy that was already present in that work, for reasons explained below.

Fig. 19 shows the normalised rate of dissipation of k by the Newtonian solvent (ε^{N^+}) and here an excellent agreement with DNS data is found except very close to the wall. This difference at the wall is a known defect of the k–ε model and exists also for Newtonian fluids. Its correction involves the use of better behaved quantities, such as the specific rate of dissipation (ω) in the so-called k–ω models, since ω is better behaved near the wall than ε. Elsewhere the predictions of $\widetilde{\varepsilon}^N$ are excellent and this is due to the inclusion of the viscoelastic destruction term (E_{τ_p}) in the transport equation of $\widetilde{\varepsilon}^N$, which decreases $\widetilde{\varepsilon}^N$ as flow viscoelasticity increases. The inclusion of a closure for E_{τ_p} improves the behaviour of $\widetilde{\varepsilon}^N$ in the logarithmic region and is also responsible for a smoother variation of the velocity profile with the Weissenberg number, which now varies monotonically with the Weissenberg number, and in particular at low We_τ, in contrast to the previous model of [9].

The predictions of the viscoelastic stress work are plotted in Fig. 20 and show that this closure is capable of capturing the lower peak in the buffer layer, a feature absent from Pinho et al.'s model [9]. As already mentioned, the differences between DNS and predictions in the viscous and buffer layers are not so important, because here the viscoelastic stress work has a negligible impact on the balance of k. However, ε^V is an important contribution to the balance of k in the inertial sublayer where it acts as a dissipative term, lowering the value of k. It would be easy to match the predictions of ε^V with the DNS data, but this would entail a higher dissipation and a concomitant reduction in k, which is already underpredicted, especially at DR = 37%. The solution of this problem is most probably the adoption of a second order closure, where the pressure strain, which must be strongly affected by the presence of the polymeric additives, is not so capable of isotropizing the Reynolds stress.

The predictions of NLT_{ij} are compared with DNS data in Fig. 21(a)–(e), including the shear component. There are some differences between the predictions and the DNS data, especially at intermediate DR, with underpredictions of peak values, but the model captures well all main features, such as the increase in NLT with DR, the shift of the peak location to higher values of y^+ as DR increases and the existence of the negative peaks of NLT_{11} in the buffer layer. All these features impact on the behaviour of NLT_{kk}, Fig. 21(e), which is part of the model for ε^V. The saturation of NLT_{kk} as DR increases to about 44% is well shown. Note, however, that the saturation of NLT_{ij} takes place in the DNS at higher We (higher DR) than that shown here, i.e., higher than the range of validity of this model. This is obvious in Fig. 21(e) where the DNS data still varies significantly between $We = 25$ and 100. In this figure we observe that the model anticipates the saturation of NLT_{ij} to lower We numbers and that the saturation value is lower than for the DNS data. This contrasts with the absence of saturation in ε^{V^+} shown in the predictions of Fig. 20, which is really a consequence of the lower value of NLT_{kk} predicted in saturation rather than a deficiency in the closure for ε^V. As a matter of fact, the closure for ε^V is quite good (cf. Fig. 14 for the behaviour of this closure in the *a priori* development phase) and shows the correct saturation if NLT_{kk} is correctly predicted. The reason this is not seen in the predictions of ε^V within the k–ε model is again rooted, we believe, on the isotropic turbulence assumption. In fact, predicting

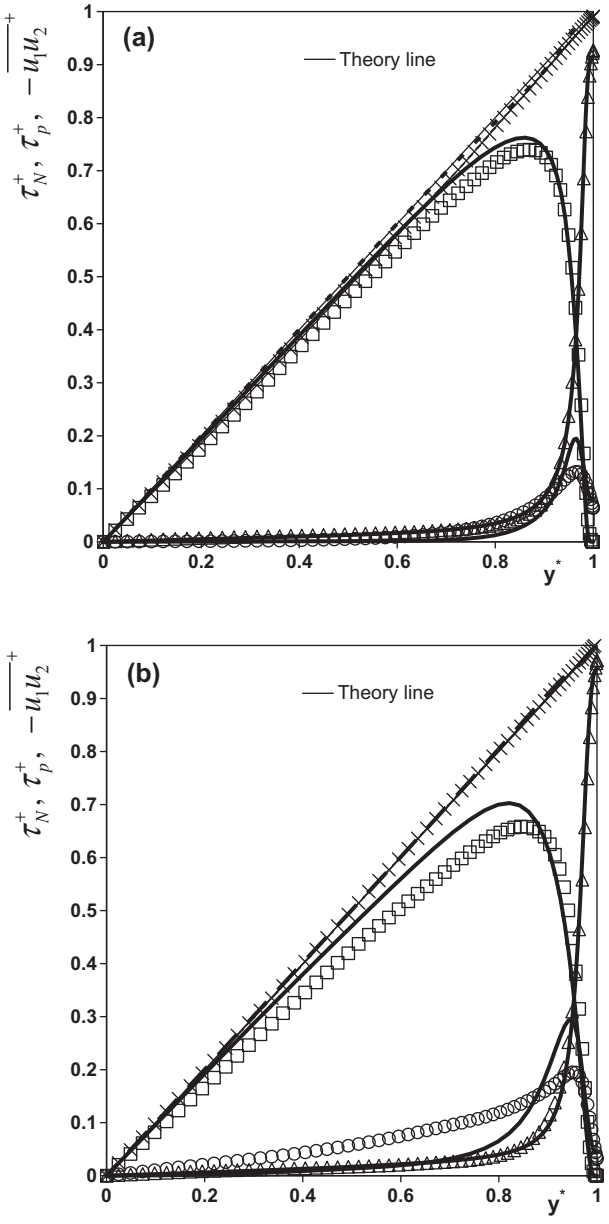

Fig. 23. Comparison between predictions (lines) and DNS data (symbols) for normalised shear stresses $(\tau_N^+, \tau_p^+, -\overline{u_1u_2}^+)$ in turbulent channel flow with $Re_{\tau 0} = 395$, $L^2 = 900$ and $\beta = 0.9$. ($\triangle$ and line) τ_N^+, ($\circ$ and line) τ_p^+, ($\square$ and line) $-\overline{u_1u_2}^+$; ($\times$ and dashed line) sum of stresses: (a) DR = 18%; (b) DR = 37%.

correctly NLT_{kk} (and ε^V) at $We = 100$ would result in excessive dissipation of k by the viscoelastic stress work at high We, i.e., k would be further underpredicted than it actually is. A compromise was reached to avoid this excessive decrease of k with We and it involved under-predicting NLT_{ij}, thus saturating it at lower NLT values and at a lower value of We, which led to a reduction of ε^V at the upper range of We.

The correct predictions of NLT_{ij} have a direct impact on the prediction of the conformation tensor, as is obvious from Eq. (11), especially regarding the two transverse normal components and the shear component (C_{22}, C_{33} and C_{12}), whereas it is not so important in the prediction of the C_{11} component, Kim et al. [35]. The profiles of C_{ij} are plotted in Fig. 22(a)–(e), and they only show improvements relative to the corresponding predictions of Pinho et al. [9] for the shear component. The quality of the comparison in C_{ij} is similar to the quality of the comparison of NLT_{ij} whenever NLT_{ij} is a major contribution to the balance of C_{ij} as for the C_{22} and C_{33} components, and is better when the impact of NLT_{ij} is smaller and C_{ij} is also determined by the other terms of the evolution equation for C_{ij} (Eq. (11)) which are exact. In addition, two terms of the RACE equation are negligible at low DR, but there are some DNS results suggesting they may need to be considered at higher and maximum drag reductions and this may improve predictions, something to be investigated in the future.

Finally it is worth analysing the distribution of all shear stresses across the channel and we do that separately for DR = 18% in Fig. 23(a) and DR = 37% in Fig. 23(b). The solvent stress is always very well captured as a consequence of the good prediction of the velocity profile and its exact definition. The Reynolds shear stress is well predicted but we always see an overprediction of the peak and an underprediction close to the wall. Since there are only three stresses, that their sum is by definition well predicted in this flow calculation and the solvent stress is correct, the compensation for the deficiencies in the Reynolds shear stress must come from an opposite deficiency in the polymer shear stress. Indeed, we observe that $\overline{\tau}_{12}^{+p}$ is overpredicted very close to the wall and underpredicted farther away as a consequence of the predictive behaviour of the shear component of the conformation tensor (C_{12}), c.f. Fig. 22(d).

7. Conclusions

A new low-Reynolds-number k–ε turbulence model is developed here for flow of dilute polymer solutions represented by the FENE-P rheological constitutive equation. The new model constitutes a major improvement over the model of Pinho et al. [9] since several of its components have been modified in light of recent DNS results. Moreover, the new model has been demonstrated to be valid for both low and intermediate drag reduction regimes.

Its main features are the new closures for the Reynolds-averaged nonlinear term of the polymer conformation equation (denoted NLT_{ij}), for the eddy viscosity, the inclusion of a viscoelastic destruction term in the transport equation of the rate of dissipation of k by the Newtonian solvent, and an extra contribution to the viscoelastic turbulent diffusion, previously neglected. Additionally, improvements were introduced in existing closures for the viscoelastic stress work model and the extension to the IDR regime.

Arguably, the most important modification was the development of the closure for NLT_{ij}, which started from its exact equation and simplification on the basis of various simplifying physical arguments, such as homogeneous isotropic turbulence, and an order of magnitude analysis. Two closures were developed for NLT_{ij}: the first closure was developed in the context of second-order turbulence models and the other, designated by "isotropic" model, considered an isotropic distribution of the Reynolds stresses and of the rate of dissipation tensor by the Newtonian solvent and is typically to be used in the context of the k–ε and k–ω turbulence models. The two models behave similarly at low drag reduction, but show differences at IDR, with the simpler model performing slightly less well. In any case both models captured the main features of the individual components of tensor NLT_{ij}, and in particular their variations with drag reduction.

The new eddy viscosity closure incorporates a polymer contribution. It behaves well, but since it is a difference between two contributions there is cause for concern and may have to be further modified when the model is tried in more complex flows in order to eliminate its inherent stability problems. The deficiencies of the previous model of Pinho et al. [9] in predicting ε^N were largely eliminated by developing a closure for the new destruction term (E_{τ_p}) appearing in the transport equation of ε^N, which accounts for the direct impact of the polymer additives. The goodness of the viscoelastic stress work (ε^V) closure developed by Pinho et al. [9] was confirmed and here this model was extended to deal with LDR and IDR. Finally, an extra term was included in the closure of the viscoelastic turbulent diffusion, which had previously been neglected at LDR.

The new turbulence model shows better predictions for all quantities, and especially for the mean velocity, the distributions of ε^N, NLT_{ij}, conformation tensor and the polymer and Reynolds shear stresses. However, the improvements in the prediction of k were small, which remains underpredicted. We think this is essentially associated to the assumption of turbulence isotropy inherent to the k–ε model. Relative to the model of Pinho et al. [9] the increase in the maximum value of k is due to the improved capacity of the new model to predict more accurately the evolution of NLT_{ij} in the buffer layer, where it captures the lower peak of NLT_{kk} profile. This impacts on the viscoelastic stress work, where it acts as a production in part of the buffer layer, thus increasing the turbulent kinetic energy. In any case, it is still necessary to address this problem, and also to improve the prediction of ε^N close to the wall, possibly on the basis of k–ω type of models.

Other discrepancies, such as the saturation of NLT_{ij} at lower values of We are also rooted on the assumption of isotropic turbulence. The link between the eddy viscosity and turbulence via $\nu_T = C_\mu \times f_\mu \times k^2/\widetilde{\varepsilon}^N$ is only through k, i.e., the reduction in Reynolds stresses accompanying DR requires a decrease in k. Therefore, there is an incompatibility between the correct variation of k, which increases, and the requirements of an eddy viscosity which must decrease with We via a decrease in k (since the variation in ε^N is not so large). A remedy within the scope of k–ε would have been to predict correctly k, but to overpredict significantly the viscous dissipation, i.e., to reduce $\nu_T = C_\mu \times f_\mu \times k^2/\widetilde{\varepsilon}^N$ by increasing $\widetilde{\varepsilon}^N$. An alternative we tested was an eddy viscosity model like $\nu_T = C_\mu \times f_\mu \times k^2/(\widetilde{\varepsilon}^N + C_2\varepsilon^V)$, which physically makes sense, but requires an extremely large (and unphysical) value of C_2. We used at the end a variation of this last option, in the sense of including a direct polymer contribution to the eddy viscosity, but as in Eq. (41). An improved relation between turbulence and the polymeric stress/conformation is required for improved modelling and there are various options. One is to make the eddy viscosity proportional to the transverse turbulence, which really decreases with We as demonstrated by Iaccarino et al. [45] in the context of the k–ε v^2-f philosophy. Another is to directly work with transport equations for the Reynolds stress or to use anisotropic k–ε models.

These options will need to be seriously considered in order to extend the model to the high and maximum drag reduction regimes and to deal with fluids having a different maximum extensibility and viscosity solvent ratio. Nevertheless it has to be emphasised that our objective of developing as general as possible viscoelastic closures for RANS models has been accomplished although not yet fully demonstrated because of the deficiency of

the adopted eddy viscosity closure, which is based on turbulence isotropy. As an example, the closure for NLT_{ij} can in principle be used within the scope of k–ε, k–ω or a 2nd order Reynolds stress model as is or with minimum changes, such as a simple recalibration of some parameter values. We did it for a k–ω model just by changing slightly the numerical values of two parameters[46].

Acknowledgments

The authors gratefully acknowledge funding from FEDER and FCT through Projects POCI/56342/EQU/2004, PTDC/EME-MFE/70186/2006 and BD/18475/2004. K.K. would like to acknowledge the support from KISTI Supercomputing Center (No. KSC-2009-S02-0013). R.S. would like to acknowledge NSF grant CBET 1055219.

Appendix I. Exact equation for NLT_{ij}

$$\overline{c_{kj}\frac{\partial u_i}{\partial x_k}+c_{ik}\frac{\partial u_j}{\partial x_k}}+\frac{\lambda}{L^2-3}\left\{-\frac{\partial C_{ik}}{\partial t}\overline{c_{mm}\frac{\partial u_j}{\partial x_k}}-\frac{\partial C_{kj}}{\partial t}\overline{c_{mm}\frac{\partial u_i}{\partial x_k}}+\left(L^2-C_{mm}\right)\left[\overline{\frac{\partial u_j}{\partial x_k}\frac{\partial c_{ik}}{\partial t}}+\overline{\frac{\partial u_i}{\partial x_k}\frac{\partial c_{kj}}{\partial t}}\right]\right\}$$
$$-\frac{\lambda}{L^2-3}\left\{\overline{c_{mm}\frac{\partial c_{ik}}{\partial t}\frac{\partial u_j}{\partial x_k}}+\overline{c_{mm}\frac{\partial c_{kj}}{\partial t}\frac{\partial u_i}{\partial x_k}}+U_n\left[\frac{\partial C_{kj}}{\partial x_n}\overline{c_{mm}\frac{\partial u_i}{\partial x_k}}+\frac{\partial C_{ik}}{\partial x_n}\overline{c_{mm}\frac{\partial u_j}{\partial x_k}}\right]\right\}$$
$$+\frac{\lambda}{L^2-3}\left\{\left(L^2-C_{mm}\right)\left[\frac{\partial C_{kj}}{\partial x_n}\overline{u_n\frac{\partial u_i}{\partial x_k}}+\frac{\partial C_{ik}}{\partial x_n}\overline{u_n\frac{\partial u_j}{\partial x_k}}\right]-\frac{\partial C_{kj}}{\partial x_n}\overline{c_{mm}u_n\frac{\partial u_i}{\partial x_k}}-\frac{\partial C_{ik}}{\partial x_n}\overline{c_{mm}u_n\frac{\partial u_j}{\partial x_k}}\right\}$$
$$+\frac{\lambda}{L^2-3}\left\{\left(L^2-C_{mm}\right)U_n\left[\overline{\frac{\partial u_j}{\partial x_k}\frac{\partial c_{ik}}{\partial x_n}}+\overline{\frac{\partial u_i}{\partial x_k}\frac{\partial c_{kj}}{\partial x_n}}\right]-U_n\left[\overline{c_{mm}\frac{\partial u_i}{\partial x_k}\frac{\partial c_{kj}}{\partial x_n}}+\overline{c_{mm}\frac{\partial u_j}{\partial x_k}\frac{\partial c_{ik}}{\partial x_n}}\right]\right\}$$
$$+\frac{\lambda}{L^2-3}\left\{\left(L^2-C_{mm}\right)\left[\overline{u_n\frac{\partial u_j}{\partial x_k}\frac{\partial c_{ik}}{\partial x_n}}+\overline{u_n\frac{\partial u_i}{\partial x_k}\frac{\partial c_{kj}}{\partial x_n}}\right]-\overline{u_nc_{mm}\frac{\partial u_i}{\partial x_k}\frac{\partial c_{kj}}{\partial x_n}}+\overline{u_nc_{mm}\frac{\partial u_j}{\partial x_k}\frac{\partial c_{ik}}{\partial x_n}}\right\}$$
$$+\frac{\lambda}{L^2-3}\left\{C_{jn}\frac{\partial U_k}{\partial x_n}\overline{c_{mm}\frac{\partial u_i}{\partial x_k}}+C_{kn}\frac{\partial U_i}{\partial x_n}\overline{c_{mm}\frac{\partial u_j}{\partial x_k}}-\left(L^2-C_{mm}\right)\left[\frac{\partial U_k}{\partial x_n}\overline{c_{jn}\frac{\partial u_i}{\partial x_k}}+\frac{\partial U_i}{\partial x_n}\overline{c_{kn}\frac{\partial u_j}{\partial x_k}}\right]\right\}$$
$$+\frac{\lambda}{L^2-3}\left\{\frac{\partial U_k}{\partial x_n}\overline{c_{mm}c_{jn}\frac{\partial u_i}{\partial x_k}}+\frac{\partial U_i}{\partial x_n}\overline{c_{mm}c_{kn}\frac{\partial u_j}{\partial x_k}}-\left(L^2-C_{mm}\right)\left[C_{jn}\overline{\frac{\partial u_k}{\partial x_n}\frac{\partial u_i}{\partial x_k}}+C_{kn}\overline{\frac{\partial u_i}{\partial x_n}\frac{\partial u_j}{\partial x_k}}\right]\right\}$$
$$+\frac{\lambda}{L^2-3}\left\{C_{jn}\overline{c_{mm}\frac{\partial u_k}{\partial x_n}\frac{\partial u_i}{\partial x_k}}+C_{kn}\overline{c_{mm}\frac{\partial u_i}{\partial x_n}\frac{\partial u_j}{\partial x_k}}-\left(L^2-C_{mm}\right)\left[\overline{c_{jn}\frac{\partial u_k}{\partial x_n}\frac{\partial u_i}{\partial x_k}}+\overline{c_{kn}\frac{\partial u_i}{\partial x_n}\frac{\partial u_j}{\partial x_k}}\right]\right\}$$
$$+\frac{\lambda}{L^2-3}\left\{\overline{c_{jn}c_{mm}\frac{\partial u_k}{\partial x_n}\frac{\partial u_i}{\partial x_k}}+\overline{c_{kn}c_{mm}\frac{\partial u_i}{\partial x_n}\frac{\partial u_j}{\partial x_k}}+C_{kn}\frac{\partial U_j}{\partial x_n}\overline{c_{mm}\frac{\partial u_i}{\partial x_k}}+C_{in}\frac{\partial U_k}{\partial x_n}\overline{c_{mm}\frac{\partial u_j}{\partial x_k}}\right\}$$
$$+\frac{\lambda}{L^2-3}\left\{-\left(L^2-C_{mm}\right)\left[\frac{\partial U_j}{\partial x_n}\overline{c_{kn}\frac{\partial u_i}{\partial x_k}}+\frac{\partial U_k}{\partial x_n}\overline{c_{in}\frac{\partial u_j}{\partial x_k}}\right]+\frac{\partial U_j}{\partial x_n}\overline{c_{mm}c_{kn}\frac{\partial u_i}{\partial x_k}}+\frac{\partial U_k}{\partial x_n}\overline{c_{mm}c_{in}\frac{\partial u_j}{\partial x_k}}\right\}$$
$$+\frac{\lambda}{L^2-3}\left\{-\left(L^2-C_{mm}\right)\left[C_{kn}\overline{\frac{\partial u_j}{\partial x_n}\frac{\partial u_i}{\partial x_k}}+C_{in}\overline{\frac{\partial u_k}{\partial x_n}\frac{\partial u_j}{\partial x_k}}\right]+C_{kn}\overline{c_{mm}\frac{\partial u_j}{\partial x_n}\frac{\partial u_i}{\partial x_k}}+C_{in}\overline{c_{mm}\frac{\partial u_k}{\partial x_n}\frac{\partial u_j}{\partial x_k}}\right\}$$
$$+\frac{\lambda}{L^2-3}\left\{-\left(L^2-C_{mm}\right)\left[\overline{c_{kn}\frac{\partial u_j}{\partial x_n}\frac{\partial u_i}{\partial x_k}}+\overline{c_{in}\frac{\partial u_k}{\partial x_n}\frac{\partial u_j}{\partial x_k}}\right]+\overline{c_{kn}c_{mm}\frac{\partial u_j}{\partial x_n}\frac{\partial u_i}{\partial x_k}}+\overline{c_{in}c_{mm}\frac{\partial u_k}{\partial x_n}\frac{\partial u_j}{\partial x_k}}\right\}$$
$$=-\frac{f(L)}{L^2-3}\left[\overline{c_{mm}\frac{\partial u_i}{\partial x_k}}\delta_{kj}+\overline{c_{mm}\frac{\partial u_j}{\partial x_k}}\delta_{ik}\right] \tag{AI-1}$$

Appendix II. Components of the NLT_{ij} tensor for the second order turbulence closure in fully developed channel flow

The NLT_{ij} model of Eq. (35), developed in Section 3.2.5, is expanded below for fully-developed channel flow for the non-zero components, which are NLT_{11}, NLT_{22}, NLT_{33} and NLT_{12} where indices 1, 2 and 3 indicate the streamwise, transverse and spanwise directions, respectively. Note that this specific closure is to be used in the context of second order turbulence models. The functions and parameters are those of Section 3.2.5.

$$NLT_{11}=C_{F1}\times\frac{C_{11}\times f(C_{mm})}{\lambda}-C_{F2}\left[2C_{21}\frac{\partial U_1}{\partial x_2}\right]$$
$$+\frac{\lambda}{f(C_{mm})}\left[\frac{C_{F3}}{C_{mm}}\times\left(2\left|\frac{\partial U_1}{\partial x_2}\right|C_{22}\frac{(\overline{u_1u_1})}{v_0}\right)\right]$$
$$-\frac{\lambda}{f(C_{mm})}\times f_{F1}\times\frac{C_{F4}}{We_{\tau0}}\times\left[2C_{22}\frac{\partial U_1}{\partial x_2}\frac{\partial U_1}{\partial x_2}\right]$$
$$+\frac{\lambda}{f(C_{mm})}\left(\frac{25}{We_{\tau0}}\right)^{0.88}\left[C_{\varepsilon_F}\frac{4}{15}\times\frac{\varepsilon^N}{v_s\times\beta}C_{mm}\times f_{F2}\right] \tag{AII-1}$$

$$NLT_{22}=C_{F1}\times\frac{C_{22}\times f(C_{mm})}{\lambda}$$
$$+\frac{\lambda}{f(C_{mm})}\left(\frac{25}{We_{\tau0}}\right)^{0.88}\left[C_{\varepsilon_F}\frac{4}{15}\times\frac{\varepsilon^N}{v_s\times\beta}C_{mm}\times f_{F2}\right] \tag{AII-2}$$

$$NLT_{33}=C_{F1}\times\frac{C_{33}\times f(C_{mm})}{\lambda}$$
$$+\frac{\lambda}{f(C_{mm})}\left(\frac{25}{We_{\tau0}}\right)^{0.88}\left[C_{\varepsilon_F}\frac{4}{15}\times\frac{\varepsilon^N}{v_s\times\beta}C_{mm}\times f_{F2}\right] \tag{AII-3}$$

$$NLT_{12}=C_{F1}\times\frac{C_{12}\times f(C_{mm})}{\lambda}-C_{F2}\left[C_{22}\frac{\partial U_1}{\partial x_2}\right]$$
$$+\frac{\lambda}{f(C_{mm})}\left[\frac{C_{F3}}{C_{mm}}\times\left(\left|\frac{\partial U_1}{\partial x_2}\right|C_{22}\frac{(\overline{u_1u_2})}{v_0}\right)\right]+\frac{\lambda}{f(C_{mm})}\left(\frac{25}{We_{\tau0}}\right)^{0.88}$$
$$\times\left[C_{\varepsilon_F}\frac{4}{15}\times\frac{\varepsilon^N}{v_s\times\beta}C_{mm}\times f_{F2}\times\left(\frac{1}{2}\frac{\partial U_1/\partial y_2}{|\partial U_1/\partial y_2|}\right)\right] \tag{AII-4}$$

References

[1] M.D. Graham, Drag reduction in turbulent flow of polymer solutions, Rheology Reviews 2 (2004) 143–170.
[2] C.M. White, M.G. Mungal, Mechanics and prediction of turbulent drag reduction with polymer additives, Annual Review of Fluid Mechanics 40 (2008) 235–256.
[3] J.M.J. Den Toonder, M.A. Hulsen, G.D.C. Kuiken, F.T.M. Nieuwstadt, Drag reduction by polymer additives in a turbulent pipe flow: numerical and laboratory experiments, Journal of Fluid Mechanics 337 (1997) 193–231.
[4] K. Gasljevic, E.F. Matthys, Experimental investigation of thermal and hydrodynamic development regions for drag-reducing surfactant solutions, Journal of Heat Transfer 119 (1997) 80–88.
[5] R. Sureshkumar, A.N. Beris, R.A. Handler, Direct numerical simulation of the turbulent channel flow of a polymer solution, Physics of Fluids 9 (3) (1997) 743–755.
[6] K.D. Housiadas, A.N. Beris, R.A. Handler, Viscoelastic effects on higher order statistics and coherent structures in turbulent channel flow, Physics of Fluids 17 (2005) 35106.
[7] R.I. Leighton, D.T. Walker, T.R. Stephens, G.C. Garwood, Reynolds stress modeling for drag-reducing viscoelastic flow, in: Joint ASME/JSME Fluids Engineering Symposium on Friction Drag Reduction, Honolulu, Hawai, USA, 2003.
[8] C.F. Li, V.K. Gupta, R. Sureshkmar, B. Khomami, Turbulent channel flow of dilute polymeric solutions: drag reduction scaling and an eddy viscosity model, Journal of Non-Newtonian Fluid Mechanics 139 (2006) 177–189.
[9] F.T. Pinho, C.F. Li, B.A. Younis, R. Sureshkumar, A low Reynolds number k–ε turbulence model for FENE-P viscoelastic fluids, Journal of Non-Newtonian Fluid Mechanics 154 (2008) 89–108.
[10] F. Durst, A.K. Rastogi, Calculations of turbulent boundary layer flows with drag reducing polymer additives, Physics of Fluids 20 (12) (1977) 1975–1985.
[11] T. Mizushina, H. Usui, Reduction of eddy diffusion for momentum and heat in viscoelastic fluid flow in a circular tube, Physics of Fluids 20 (10) (1977) S100–S107.
[12] M.R. Malin, Turbulent pipe flow of power-law fluids, International Communications in Heat Mass Transfer 24 (7) (1997) 977–988.
[13] M.R. Malin, Turbulent pipe flow of Herschel–Bulkley fluids, International Communications in Heat Mass Transfer 25 (3) (1998) 321–330.
[14] F.T. Pinho, A GNF framework for turbulent flow models of drag reducing fluids and proposal for a k–ε type closure, Journal of Non-Newtonian Fluid Mechanics 114 (2003) 149–184.
[15] D.O.A. Cruz, F.T. Pinho, Turbulent pipe flow predictions with a low Reynolds number k–ε model for drag reducing fluids, Journal of Non-Newtonian Fluid Mechanics 114 (2003) 109–148.
[16] D.O.A. Cruz, F.T. Pinho, P.R. Resende, Modeling the new stress for improved drag reduction predictions of viscoelastic pipe flow, Journal of Non-Newtonian Fluid Mechanics 121 (2004) 127–141.
[17] P.R. Resende, M.P. Escudier, F. Presti, F.T. Pinho, D.O.A. Cruz, Numerical predictions and measurements of Reynolds normal stresses in turbulent pipe flow of polymers, International Journal of Heat and Fluid Flow 27 (2006) 204–219.
[18] F.T. Pinho, B. Sadanandan, R. Sureshkumar, One equation model for turbulent channel flow with second order viscoelastic corrections, Flow, Turbulence and Combustion 81 (2008) 337–367.
[19] C.D. Dimitropoulos, R. Sureshkumar, A.N. Beris, R.A. Handler, Budgets of Reynolds stress, kinetic energy and streamwise enstrophy in viscoelastic turbulent channel flow, Physics of Fluids 13 (4) (2001) 1016–1027.
[20] C.D. Dimitropoulos, R. Sureshkumar, A.N. Beris, Direct numeric simulation of viscoelastic turbulent channel flow exhibiting drag reduction: effect of variation of rheological parameters, Journal of Non-Newtonian Fluid Mechanics 79 (1998) 433–468.
[21] B. Yu, Y. Kawaguchi, Parametric study of surfactant-induced drag-reduction by DNS, International Journal of Heat and Fluid Flow 27 (2006) 887–894.
[22] P.K. Ptasinski, B.J. Boersma, F.T.M. Nieuwstadt, M.A. Hulsen, B.H.A.A. Van Den Brule, J.C.R. Hunt, Turbulent channel flow near maximum drag reduction: simulation, experiments and mechanisms, Journal of Fluid Mechanics 490 (2003) 251–291.
[23] V.K. Gupta, R. Sureshkumar, B. Khomami, Polymer chain dynamics in Newtonian and viscoelastic turbulent channel flows, Physics of Fluids 16 (2004) 1546–1566.
[24] Q. Zhou, R. Akhavan, A comparison of FENE and FENE-P dumbbell and chain models in turbulent flow, Journal of Non-Newtonian Fluid Mechanics 109 (2003) 115–155.
[25] G.V. Reddy, R.P. Singh, Drag reduction effectiveness and shear stability of polymer–polymer and polymer–fibre mixtures in recirculatory turbulent flow of water, Rheologica Acta 24 (1985) 296–311.
[26] V.N. Kalashnikov, Degradation accompanying turbulent drag reduction by polymer additives, Journal of Non-Newtonian Fluid Mechanics 103 (2002) 105–121.
[27] Y. Dubief, C.M. White, V.E. Terrapon, E.S.G. Shaqfeh, P. Moin, S.K. Lele, On the coherent drag reducing and turbulence enhancing behaviour of polymers in wall flows, Journal of Fluid Mechanics 514 (2004) 271–280.
[28] C.D. Dimitropoulos, Y. Dubief, E.S.G. Shaqfeh, P. Moin, S.K. Lele, Direct numerical simulation of polymer-induced drag reduction in turbulent boundary layer flow, Physics of Fluids 17 (2005) 11705.
[29] W. Li, X. Li, M.D. Graham, Non-linear travelling waves as a framework for understanding turbulent drag reduction, Journal of Fluid Mechanics 565 (2006) 353–362.
[30] R. Leighton, D. Walker, S. Todd, Reynolds stress modeling for drag reducing viscoelastic flows, in: Proceedings of the 55th Annual Meeting of the American Physical Society, Division of Fluid Dynamics, Austin, Texas, 2002.
[31] E.S. Shaqfeh, G. Iaccarino, M. Shin, A RANS model for turbulent drag reduction by polymer injection and comparison with DNS, in: Proceedings of the 78th Annual Meeting of The Society of Rheology, Portland, Maine, 2006.
[32] P.A. Durbin, Application of a near-wall turbulence model to boundary layers and heat transfer, International Journal of Heat and Fluid Flow 14 (1993) 316–323.
[33] B.A. Younis, T.B. Gatski, C.G. Speziale, Towards a rational model for the triple velocity correlations of turbulence, Proceedings of the Royal Society of London 456 (2000) 909–920.
[34] B.A. Younis, C.G. Speziale, T.T. Clark, A rational model for the turbulent scalar fluxes, Proceedings of the Royal Society of London 461 (2005) 575–594.
[35] K. Kim, R.J. Adrian, S. Balachandar, R. Sureshkumar, Dynamics of hairpin vortices and polymer-induced turbulent drag reduction, Physical Review Letters 100 (2008) 134504.
[36] S.B. Pope, Turbulent Flows, Cambridge University Press, Cambridge, UK, 2000.
[37] H. Schlichting, K. Gersten, Boundary Layer Theory, eighth ed., revised and enlarged., Springer, Heidelberg, 2000.
[38] F.T. Pinho, Time-average double correlations in turbulence models of FENE-P viscoelastic fluids, Internal report, project FCT POCI/EQU/56342/2004, FEUP, Porto, 2005.
[39] J. Mathieu, J. Scott, An Introduction to Turbulent Flow, Cambridge University Press, Cambridge, UK, 2000.
[40] W.P. Jones, B.E. Launder, The prediction of laminarization with a two-equation model of turbulence, International Journal of Heat and Mass Transfer 15 (1972) 301–314.
[41] Y. Nagano, M. Hishida, Improved form of the k–ε model for wall turbulent shear flows, Journal of Fluids Engineering 109 (1987) 156–160.
[42] E.R. Van Driest, On turbulent flow near a wall, Journal of Aeronautical Sciences 23 (1956) 1007–1011.
[43] Y. Nagano, M. Shimada, Modeling the dissipation-rate equation for two-equation turbulence model, in: Ninth Symposium on Turbulent Shear Flows, Kyoto, Japan, 1993.
[44] T.S. Park, H.J. Sung, A nonlinear low-Reynolds-number κ–ε model for turbulent separated and reattaching flows-I. Flow field computations, International Journal of Heat and Mass Transfer 38 (14) (1995) 2657–2666.
[45] G. Iaccarino, E.S.G. Shaqfeh, Y. Dubief, Reynolds-averaged modeling of polymer drag reduction in turbulent flows, Journal of Non-Newtonian Fluid Mechanics 165 (2010) 376–384.
[46] P.R. Resende, F.T. Pinho, B.A. Younis, K. Kim, R. Sureshkumar, Development of a k–ω turbulence model for FENE-P fluids, in: J.C.F. Pereira, A. Sequeira (Eds.), Paper 1400 in Proceedings of the Vth European Conference on Computational Fluid Dynamics, ECCOMAS CFD, Lisbon, Portugal, 14–17 June, 2010.